International Journal of Social Robotics (2024) 16:2109–2132
https://doi.org/10.1007/s12369-024-01169-3

Through-Window Home Aerial Delivery System with In-Flight Parcel Load and Handover: Design and Validation in Indoor Scenario

Alejandro Suarez[1] · Antonio Gonzalez[1] · Carlos Alvarez[1] · Anibal Ollero[1]

Accepted: 16 July 2024 / Published online: 1 October 2024

Abstract

This paper presents the design, development, and validation in indoor scenario of an aerial delivery system intended to conduct the delivery of light parcels directly to the user through the window of his/her home, motivated by the convenience of facilitating the access to medicines to people with reduced mobility.The system consists of a fully-actuated multi-rotor (FAMR) equipped with a front basket where the parcel to be delivered is loaded by a lightweight and compliant anthropomorphic dual arm system (LiCAS) located at the supply point, using one of the arms to drop the parcel in the basket while the other arm holds its base to support the sudden moment exerted at the FAMR. The paper analyses four types of physical interactions raised during the operation on flight: (1) sudden changes in the mass distribution of the FAMR during the load/unload phase, affecting the multi-rotor position-attitude controllers, (2) impact and impulsive forces exerted by the human on the FAMR to demonstrate the reliability and robustness of conventional cascade controllers, (3) passive accommodation of the LiCAS while holding the FAMR during the parcel load, relying on the mechanical joint compliance, and (4) compliant human–FAMR interaction, interpreting the multi-rotor pose control error as a Cartesian/angular deflection to implement an admittance controller that allows the user guiding the platform. Experimental results allow the identification and characterization of these effects for different payload masses. The execution of the complete operation, involving the parcel load with the LiCAS and handover by the user through a window, is validated in a representative indoor scenario.

✉ Alejandro Suarez
asuarezfm@us.es

Antonio Gonzalez
mantonio@us.es

Carlos Alvarez
carlosacia2@gmail.com

Anibal Ollero
aollero@us.es

[1] GRVC Robotics Laboratory, Universidad de Sevilla, Camino de los Descubrimientos s/n, 41092 Seville, Spain

Graphical Abstract

Keywords Home aerial parcel delivery · Human–aerial robot interaction · Robot–robot interaction · Compliance

1 Introduction

Providing fast response and continuous service of medicine delivery to people at home is highly desirable in emergency situations in urban or rural environments [1–4], particularly at night when the availability of health centers and pharmacies is lower. Furthermore, the increasing aging of the world's population along with the high rates of people of reduced mobility makes necessary the development of novel solutions for delivering light parcels such as medicines directly to the user's home [5]. Given the complexity and density of obstacles typical of urban environments [6, 7], and despite the significant advances in autonomous navigation of ground robots [8–13], these platforms may not be suitable for fast operation, taking also into account the difficulties or impossibility of accessing the interior of the buildings, particularly in multi-storey buildings. In this sense, aerial robots can benefit from their ability to fly and reach the user's home through its window, avoiding all these inconveniences, while contributing to the comfort of the users who can receive directly the parcel [14], at expenses of providing lower payload capacity and flight time compared to ground platforms [15, 16]. What should be further investigated is the physical interaction of the human user with the aerial platform during the aerial delivery operation [17–19], taking into account that the flight controller should be robust to sudden changes in the payload as well as to pushing/pulling forces exerted by the human user [20, 21]. What is more, the combination of aerial robots with collaborative ground manipulators [22, 23] integrated in human workspaces allows the realization of autonomous parcel load and delivery operations [24]. This is the main concept of the aerial delivery system developed in this work, depicted in Fig. 1.

Fig. 1 Through-window aerial delivery system consisting of fully actuated multi-rotor (FAMR) and lightweight and compliant anthropomorphic dual arm system (LiCAS) located in the supply area used to load the parcel in the FAMR with the left arm while the right arm holds the basket base

1.1 Practical Issues in Aerial Parcel Delivery

Although the use of drones for last mile parcel delivery is quite extended nowadays, there exist relevant practical and safety issues that limit this application in dense urban environments [25], like most cities and mid size towns. First of all, unless the parcel is dropped or detached from a cable [26–30], the aerial platform should land in an area specifically enabled for it [31], possibly on the roof of the buildings to avoid interfering with the pedestrians or the road traffic. This solution can be suitable and adopted in hospitals and some markets dealing with light loads such as bookstores or clothes shops, but it constraints the access of the parcel for the people in general. What is more, this is not ergonomically comfortable as the user should bend down to pick up the parcel from the floor. Second, the potential damage that an aerial delivery platform flying in urban environment might cause increases considerably with its weight [32], which is basically determined by the payload capacity. Thus, it is preferable to deploy relatively low weight drones in terms of safety [33], taking into account however that the integration of on-board sensors and devices for navigation [34, 35] such as cameras, LiDAR, computers, batteries, the payload itself and the delivery mechanism, impose a typical minimum overall weight in the range of hundreds of grams or few kilograms. Third, considering human-centered aspects, the aerial robot should be able to interact safely with the user, providing a certain level of multi-modal accommodation during the delivery task, in terms of gesture recognition and, more importantly, physical interaction on flight [20, 36].

1.2 Design of Aerial Delivery Robots

Literature review on aerial delivery robots [37] evidences a wide variety of mechanisms and platforms designed for this purpose, consisting of small-medium scale multi-rotors equipped with grippers [38] or robotic arms [39]. Three configurations can be distinguished depending on whether the parcel is attached at the base of the aerial platform [24, 40, 41], grasped by the manipulator [39], or if it is suspended from a cable [27–29]. The aerodynamic influence of the parcel location on the multi-rotor platform is analyzed in [41], whereas [42] proposes an adaptive controller to compensate variations in the position of the carried load when this is not correctly secured. The undesired swing effect of cable suspended loads requires the design of trajectory generation and tracking control methods as described in [43]. Reference [18] presents the design of a cable suspended dual arm aerial manipulator intended to deliver hand tools to human operators working on high altitude power lines (aerial handover), separating the arms from the multi-rotor base to increase the separation distance between the human and the propellers. Protecting the user from the proximity of the propellers is also critical to prevent injuries [44], which typically involves introducing light shielding structures that reduce the effective payload capacity of the aerial platform. In case the aerial delivery operation is conducted on flight with robotic manipulators rigidly attached to the multi-rotor base, it is necessary to account for the interaction forces that the human user may exert on the multi-rotor [21] when grasping the parcel.

Among the diverse configurations and morphologies of aerial platforms that can be designed [45], fully actuated multi-rotors (FAMR) [46, 47] are particularly suitable for the intended application due to their ability to decouple the position and attitude control, since it could result uncomfortable for the user if the parcel is tilting while the platform is changing its position during the handover operation. More importantly, it is highly desirable that the aerial platform is able to maintain its position despite the user may exert tilting moments in the platform that could lead to a collision as may occur with co-planar configurations due to the coupled dynamics. Note however that the maximum tilting angle that fully actuated multi-rotors can reach while maintaining the position fixed is limited (around 10–20 deg) and determined by the configuration of the rotors in the frame structure, being a trade-off with the maximum horizontal force that can be generated while maintaining the attitude fixed.

1.3 Lightweight and Compliant Manipulators for Parcel Load

The problem of loading the aerial robot with the parcel to be delivered can be solved in two ways [37]. On the one hand, the aerial robot can be equipped with a grasping mechanism or manipulator capable to take the parcel from the supply point, becoming an aerial robotic manipulator [39]. Although the weight of simple grippers [48] and other grasping mechanisms [38] is relatively low, the convenience of incorporating these is affected by three factors: the reduction of the effective payload capacity due to the added weight, the lack of reach of grippers that impose a high positioning accuracy of the aerial platform for grasping the load (if this can be accessed), and the aerodynamic downwash interaction with moving objects underneath if these are not properly grabbed at the supply point. On the other hand, the aerial robot can benefit from the dexterous manipulation capabilities of robotic arms located at the supply point used to load the parcel and even assist the aerial platform in the landing maneuver [49, 50].

Taking into account the convenience of deploying low weight aerial platforms in dense urban areas due to safety reasons, the weight of the payload will be limited to few grams or hundreds of grams, so very low weight robotic manipulators are more suitable for this purpose [51, 52] than heavy industrial manipulators with high payload capacity, which contributes to reduce implementation costs and facilitates their integration in human workspaces. Mechanical joint compliance is a highly convenient feature for a robotic manipulator physically interacting with an aerial platform on flight since the passive accommodation provides a certain tolerance to position deviations [53]. A compliant dual arm also allows to conduct bimanual manipulation tasks in close kinematic chain, using for example one of the arms for grabbing while the other executes the task [54], as shown in Fig. 1.

1.4 Human–Robot Interaction (HRI)

The aerial delivery of a parcel using a drone is expected to be a fast operation involving both visual [55] and physical [56] interaction between the human user and the robot, so the handover can be performed in a natural and intuitive way for the customer, taking into account that nowadays people is not familiar to this kind of service. Therefore, it is expected that users tend to adopt behaviours and gestures typically employed when interacting with a delivery man/woman. The noise generated by multi-rotor propellers when flying makes verbal communication between the human and the aerial robot less convenient [57, 58]. Therefore, communication between the aerial robot and the human should rely mainly on visual signals and gestures, and possibly through simple graphical user interfaces displayed on the mobile phone of the user, for example to confirm that he/she is the recipient of the parcel. Deep learning methods have been applied in [59] for recognizing hand gestures to control multi-rotors, whereas reference [60] implements in real-time a method for the detection of body and hand gestures for rescue UAVs (Unmanned Aerial Vehicles). A survey on gesture languages for human–UAV interaction is presented in [61]. Reference [62] provides a large dataset of aerial images taken by a multi-rotor in urban-rural environments in different conditions, to be used for benchmarking human behaviours models developed for UAVs.

Several safety aspects in physical human–robot interaction were addressed in [63], from the early design phase of the robot, the consideration of faults and possible injuries that may arise, and the use of benchmarks for evaluating robots performance. Reference [56] also provides an overview on safe physical HRI, involving design and development principles for compliant robot manipulators, comprising the mechatronics, control, and motion planning. Few works present experimental results of aerial robots physically interacting on flight with humans due to the well-motivated concerns in terms of safety and stability [17, 18, 20, 21]. An early work on physical human–quadrotor interaction was presented in [17], proposing an admittance controller to allow the user guiding the platform by exerting contact forces. Authors in [20] consider the physical human–robot interaction to address the problem of guiding a human through the forces exerted by a tethered multi-rotor. Aerial tool delivery (handover) to human workers in the context of power-line maintenance operations was firstly presented in [18], using cable-suspended aerial manipulators to increase safety with respect to solutions in which the manipulator is attached to the multi-rotor base [21]. It is expected that non expert human users may exert (intentionally or not) wrenches that might destabilize the aerial platform controller [64], causing a potential crash, and what is worst, injury the people. However, as occurred with industrial robotic arms that were traditionally isolated in cages to prevent the accidental interaction with human workers and that later raised the concept of collaborative robots, aerial robots should be also able to interact closely with the people, involving a certain ability to support impacts, collisions, or pushing forces.

1.5 Main Contribution and Novelties

This paper presents the design, development, and experimental validation of an aerial delivery system, depicted in Fig. 1, consisting of a lightweight and compliant anthropomorphic dual arm system (LiCAS) that supplies with light parcels such as medicines a fully actuated multi-rotor (FAMR) capable to deliver them directly to the user's home through the window of her/his building. The paper considers two types of interactions:

1. Physical interaction between the LiCAS and the FAMR during the parcel load phase conducted on flight, using one of the arms of the LiCAS to hold the basket of the FAMR while the other arm drops the parcel.
2. Human–FAMR interactions on flight, including impulsive forces and perturbations in grabbing situations, as well as interaction forces exerted by the user to guide the aerial platform during the handover operation.

Position and attitude deviations experimentally identified in the FAMR when the parcel is dropped in the basket will be supported by the holding arm, exploiting the passive accommodation capability of the LiCAS manipulator to help the multi-rotor controller to compensate the exerted moment due to the mass unbalance. The stability and reliability of the implemented attitude-position cascade controller to different perturbations exerted by the human user is also experimentally evaluated. A human–aerial robot interaction control scheme that allows the user guiding the platform by hand is proposed, relying on the translational and rotational decoupling of the fully actuated multi-rotor along with a deflection interpretation of the position/attitude control error of the platform to implement an admittance controller. The complete parcel load and delivery operation is validated in a representative indoor testbed equipped with an Opti-Track positioning system.

The key innovation aspects comprised in this work are therefore the following:

- The intended application involving parcel delivery on flight through the window of the users' home, describing the proposed design concept and involved interactions.
- The development of the aerial delivery system comprising the FAMR and the LiCAS dual arm manipulator, along with the implemented control schemes.
- The problem of loading a parcel in the aerial platform while hovering, relying on the mechanical compliance of the manipulator to support the position/attitude deviations of the multi-rotor.
- The experimental evaluation of the different interactions previously mentioned, as well as the system validation in an indoor testbed.

The rest of the paper is organized as follows. Section 2 presents the intended application, describing in Sect. 3 the developed system. Section 4 is focused on system modelling, whereas Sect. 5 covers the controller design. Experimental results are provided in Sect. 6, reporting the conclusions of the paper in Sect. 7.

2 Problem Statement

2.1 Intended Application

One of the goals of the European Robotics and AI Network (euROBIN, [65]) in which this work is framed is the development of outdoor aerial robots that can contribute to achieve more sustainable communities. Motivated by the recent situation of confinement, and more generally, with the aim to assist people with certain mobility limitations, this work considers the problem of aerial delivery directly to the user at home through the window. Unlike the window-docking delivery drone presented in [66], that requires a perching platform installed under the customer window, the approach considered in this work consists in conducting the through-window delivery on flight in order to reduce the involved time and mechanisms required for perching, exploiting the control capabilities of fully actuated multi-rotor platforms [67] and adopting human-centered aspects such that the aerial delivery operation results comfortable and safe for the user.

The aerial robot presented in this work is intended to conduct the delivery of light loads (less than 0.5 kg) in urban or rural environments directly to the customers' home, using the window as interface element and reference frame for the operation. The proposed concept design, illustrated in Fig. 2, aims to make the reception of small packages, such as medicines or envelopes, more comfortable for users, particularly those with reduced mobility. The envisioned operation consists of five phases: (1) the aerial robot takes-off from the supply point, either a logistic center or a delivery truck, where a robotic manipulator will load the parcel to be delivered, (2) the aerial robots navigates outdoors to reach the house or building of the customer [25, 68], (3) the robot approaches to the designated window in the facade of the building, using visual, visual-inertial, LiDAR, or other sensors [69, 70] for accurate positioning relative to the window frame, until the package is close enough to the window, (4) the user retrieves the parcel on flight, involving the physical interaction with the aerial platform [47, 71, 72], and (5) the platforms navigates back to the supply point and lands. The paper is focused on the first and fourth phases. The approach of conducting the delivery operation on flight is justified due to the convenience of avoiding the installation on perching mechanisms on the facade of the user [66] and reducing the time and complexity of conducting the perching maneuver, considering also the case in which the parcel has to be loaded on flight on the drone due to time or space constraints.

2.2 General Design Requirements

The home aerial delivery robot should be designed considering, among others, the following practical aspects:

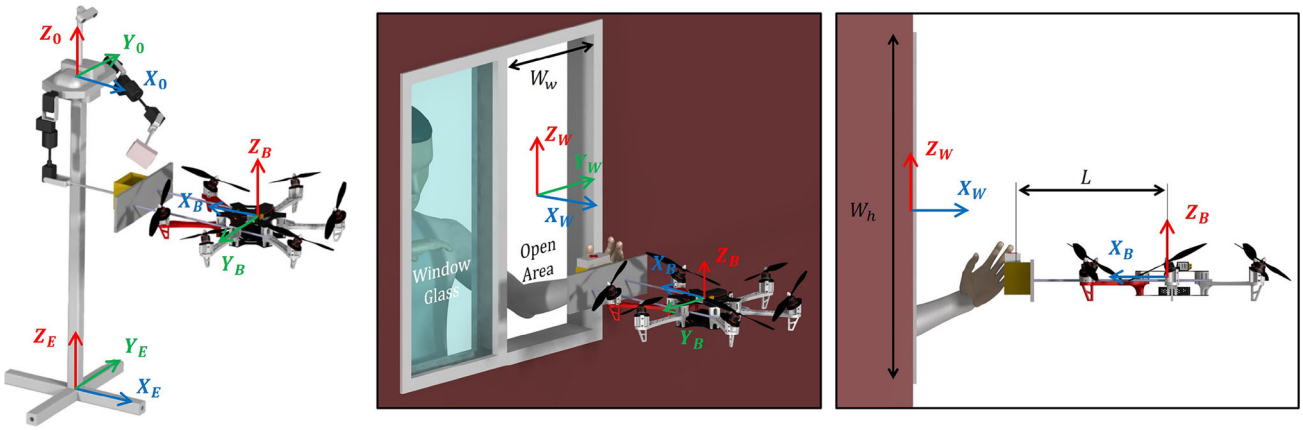

Fig. 2 Through-window home aerial delivery concept. Left: the lightweight and compliant anthropomorphic dual arm system (LiCAS) loads the parcel on the basket of the fully actuated multi-rotor (FAMR), holding its base with the right arm to support the instantaneous mass unbalance. Right: the FAMR hovers in front of the window so the user can retrieve the parcel

- *Size and weight of the platform* the risk and potential injuries that drones may cause on people or the environment flying in urban environments in case of fault make particularly necessary to reduce as much as possible the overall weight of the aerial robot, at expenses of providing limited payload capacity and removing not strictly necessary mechanisms such as grippers.
- *Maximum payload capacity* related to previous point, the mass of the load in the considered application will be in the range of few grams or hundreds of grams, which is still suitable for the transportation of light loads such as medicines, envelopes, clothes, or food. The maximum payload is also limited by the tilting moment due to the mass unbalance, since the parcel must be out of the perimeter of the propellers, as depicted in Fig. 2
- *Control of physical interactions with humans* since the parcel delivery operation will be conducted on flight, the multi-rotor controller should be able to account for pushing or pulling forces exerted by the user when retrieving the parcel from the basket, ensuring stability of the position and attitude controller despite the uncertainty in the magnitude, direction and pattern of wrenches exerted by users.
- *Shielding rotors for safety* since the FAMR will maintain almost constant its heading relative to the human user during the approaching and delivery phases (see Fig. 2), a simple shielding frame in the front part of the platform separating the basket from the propellers is enough to reduce the risk of injury during the handover, avoiding the need of shielding the entire platform and the consequent weight.
- *On-board perception for detection and localization* the limited reach of the users' hand when retrieving the parcel through the window from the basket makes necessary the implementation of accurate vision-based position estimation methods that allow the detection and localization of the window frame and the identification of human gestures [73]. Alternatively, adhesive visual marker [74] could be put in the window to facilitate its localization.

These general requirements motivate the design and development of the FAMR platform presented in next section.

3 Developed System

3.1 FAMR Platform Description

The aerial platform used in this work is based on the extensively used F550 hexarotor frame, which has been modified with 3D printed parts to integrate the autopilot, electronic speed controllers, and the rest of on-board components indicated in Fig. 3. The propulsion system consists of six DJI 2312E rotors with 9 × 4.5 inch propellers, and the XRotor 40A electronic speed controllers (ESC). The hexarotor is equipped with a Raspberry Pi 3 Model B board connected to the Emlid's sensors shield Navio2 autopilot executing the Ardupilot flight controller. The platform is powered by a 5000 mAh 4 S LiPo battery providing 10 min flight time. The main specifications are summarized in Table 1. Note that the adoption of a hexarotor platform instead of a standard quadrotor, although involving higher cost and weight, presents two relevant benefits. On the one hand, the possibility to translate without tilting results in more comfortable interactions for the human user when grasping the parcel. On the other hand, it provides redundancy in the actuators that can be exploited for fault tolerance, which is particularly relevant when flying in urban scenarios.

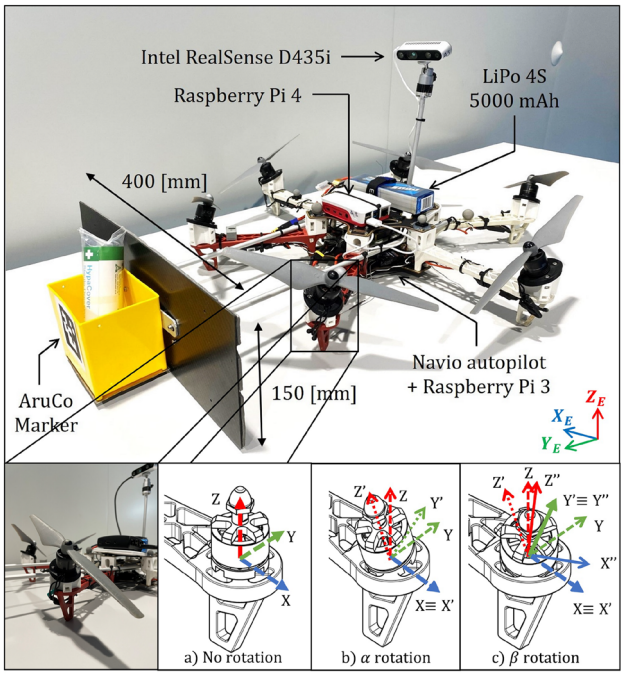

Fig. 3 Fully-actuated platform for through-window delivery (up) and sequence of rotations of the propellers (down)

The FAMR incorporates a delivery basket (100 × 90 × 80 mm size) located at $L_b = 500$ mm from the geometric center of the hexarotor frame, supported by a 400 × 150 × 1.5 mm carbon fiber frame that protects the user from the propellers. This frame is attached to the multi-rotor base through a pair of aluminum rods, responsible of transmitting the external wrenches exerted by the human user to the aerial platform. The basket is located out of the perimeter of the multi-rotor to avoid that the user may be injured by the propellers. Note that carrying the parcel on top or bottom of the multi-rotor makes the handover more difficult and risky for the customer. Parcels bigger than medical packages can be also transported as long as they do not interfere with the airflow of the propellers and can be retrieved safely through the front protection panel. An Intel RealSense D435i camera is also incorporated for visual detection and localization of the supply and delivery points, integrating another Raspberry Pi 4 computer for on-board image processing. Since the FAMR platform is built with standard components commercially available and widely used in aerial robotics, the proposed design is useful in the sense that it provides an initial estimation of the manufacturing cost and the main features of the home aerial delivery platform in terms of weight, flight time, payload capacity, and energy consumption [75].

The fully-actuated configuration is achieved by tilting the brushless motors of the propellers using two different 3D printed parts that perform two successive rotations, as represented in Fig. 3: a first rotation α_k around the X-axis of the

Table 1 Main features of the fully actuated multi-rotor

Parameter	Value
Weight/payload	2.75/1.0 kg
I_{XX}	0.03 kg m^2
I_{YY}	0.03 kg m^2
I_{ZZ}	0.054 kg m^2
Propellers	DJI 9 × 4.5 inch
Brushless motors	DJI 2312E
LiPo Battery	4 S, 5000 mAh
Max. F_X/F_Y	0.40/0.55 kg
Max. weight in the basket	0.15 kg

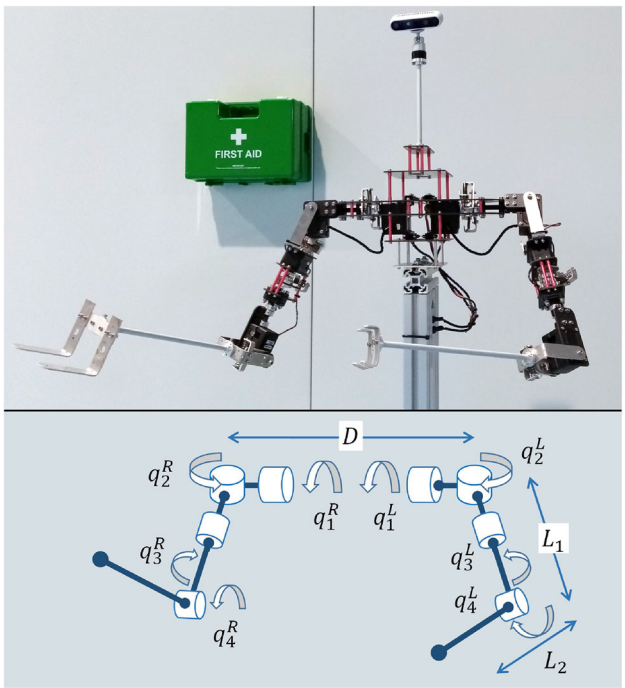

Fig. 4 Up: Lightweight and compliant anthropomorphic dual arm system (LiCAS) used to load the parcel on the FAMR, holding the basket with the right arm while the left arm drops the parcel. Down: kinematic model of the LiCAS

XYZ base of the propeller, and then a rotation β_k around the Y'-axis of the new XYZ' base. Based on [76], the values chosen for the angles α and β are as follows: $\alpha_k = -(-1)^k 20°$ and $\beta_k = (-1)^k 20°$, for $k = 1, 2, \ldots, 6$.

3.2 LiCAS Dual Arm

The manipulator used to load the parcel in the front basket of the fully actuated multi-rotor is the lightweight and compliant anthropomorphic dual arm system (LiCAS) shown in Fig. 4. This is a human-size and human-like manipulator derived from our previous works in aerial robotic manipulation [51, 52], and whose main features are summarized in Table 2.

Table 2 Main features of the LiCAS manipulator

Parameter	Value
Weight/payload	2.5/0.7 kg
Upper arm link length (L_1)	250 mm
Forearm link length (L_2)	250 mm
Separation between arms (D)	360 mm
Max. joint speed	250 deg/s
Max. joint deflection	15 deg
Joint stiffness	5–15 Nm/rad
Power supply	12–16 V

The control capabilities of the arms are determined by the smart servo actuators [51, 52], providing joint position and speed feedback and control at a maximum rate around 70 Hz, determined by the serial interface. The arms are built with smart servo actuators, supported by a customized frame structure manufactured in carbon fiber and aluminum, specifically designed to be very lightweight but highly rigid and resistant to impacts, introducing a spring-lever transmission mechanism between the actuators shaft and the links to provide mechanical joint compliance, as depicted in Fig. 5. The end effector of the right arm has been equipped with two electromagnets pointing upwards used to hold the metallic frame at the base of the basket, as depicted in Fig. 1. The left arm incorporates a simple hook-like frame used to grasp from the handle and drop the parcel on the basket.

Although the LiCAS manipulator employed here for parcel load was initially developed for aerial robotic manipulation, this dual arm system is suitable for its integration in human-shared environments like pharmacies due to their mechanical features, since its very low weight and joint compliance make it intrinsically safe and easy to install on fixed base or in linear platforms typical of vertical storage solutions. Additionally, its cost is approximately one order of magnitude lower compared to industrial robotic arms built with Harmonic Driver gears and more expensive mechanical components, taking into account that the intended application does not require the high level of positioning accuracy or payload capacity provided by industrial manipulators.

3.3 System Architecture

The components and architecture of the proposed aerial delivery system design are represented in Fig. 6, comprising the FAMR, the LiCAS, and the Ground Control Station (GCS).

The LiCAS dual arm manipulator, located at the supply point, either a delivery truck or an indoor facility, consists of a series of smart servo actuators for end effector positioning

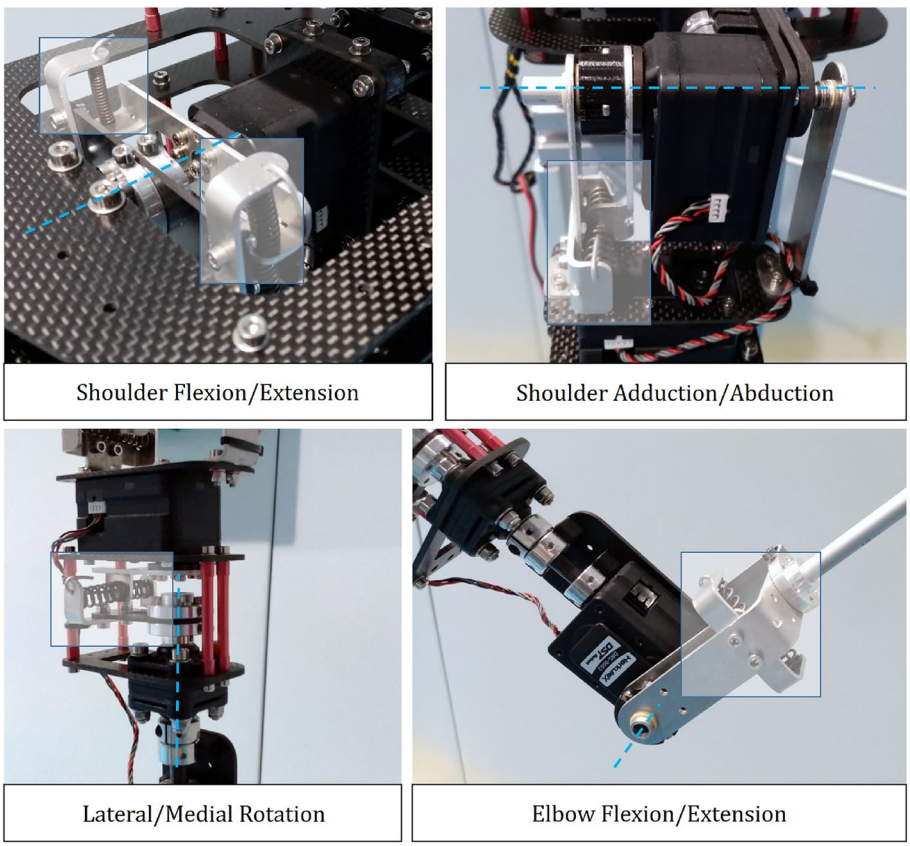

Fig. 5 Compliant spring-lever transmission mechanism integrated in the four joints of the LiCAS

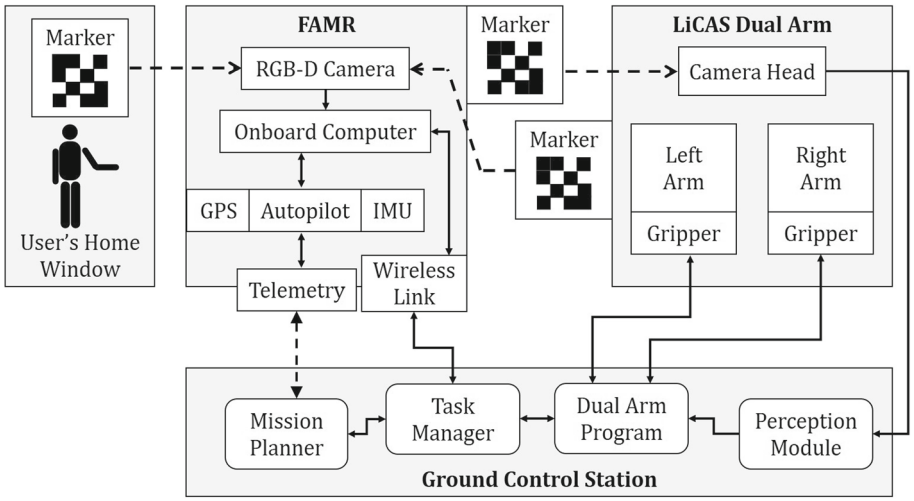

Fig. 6 Components and architecture of aerial delivery system with FAMR platform and LiCAS dual arm manipulator for parcel load

and orientation [51, 52] connected in daisy chain to the GCS computer where the Dual Arm Control Program is executed. One of the arms will be equipped with a gripper for grasping and dropping the parcel on the FAMR basket, while the other grasping mechanism will be used for grabbing and holding the basket on flight to prevent the FAMR displacement when the parcel is dropped. A camera head as the one depicted in Fig. 4 will be used to detect and accurately localize the marker [74] attached to the front part of the basket (see Fig. 3) so the arms can compensate and correct position deviations of the FAMR when conducting the parcel load operation.

The FAMR platform, besides the autopilot and the GNSS (Global Navigation Satellite System) position sensor for outdoor navigation, integrates a camera as shown in Fig. 3 also for detecting and localizing the markers attached to the LiCAS manipulator in the supply point, and the marker that the user should put in his/her window to facilitate the approaching and aerial delivery operation. Given the limited computational power of small computer boards suitable for integration in aerial platforms such as Rasperry Pi, simple but effective marker detection methods should be implemented [74] for relative positioning of the platform with respect to the manipulator during the parcel load phase, or with respect to the window during the aerial delivery. Taking into account that GNSS sensors have estimation errors in the range of 2 m, it is desirable that the perception system provides minimum detection and localization range around 5 m.

The GCS executes the Task Manager, the main software module that handles the aerial delivery operation involving the FAMR and the LiCAS manipulator, relying on the Mission Planner for generating and monitoring the flight plan, as well as the Dual Arm Control Program and the perception modules for detection and localization.

3.4 Safety Aspects in Aerial Parcel Delivery

The proposed application of aerial parcel delivery through the window involves certain risks that must be carefully considered during the experimental evaluation reported in Sect. 6, or towards the real application outdoors. Although the necessary conditions and requirements for flying outdoors in urban environments depend on the particular regulation framework of each country, region or state, it is possible to distinguish two main safety issues associated to the aerial platform. On the one hand, and possibly the most critical, the risk of crash of the multi-rotor during the navigation phase or while hovering in front of the user's home may have severe consequences in case of impact against pedestrians, resulting on serious injuries or even death if the energy of the impact is above 40 Joules.[1] References [33, 77, 78] analyze the possible damages that drones may cause depending on their mass, stating that for weights under 250 gs these platforms are harmless, but above 2 kg and few meters height consequences may be fatal. Therefore, flying at minimum altitude possible without interfering road traffic and reducing the overall mass are critical requirements, requiring for this the miniaturization of the on-board electronics and sensors (which is out of the scope of this work). On the other hand, shielding the multi-rotor propellers in order to prevent the impact against the hand, face, neck, or any other exposed part of the user's body that could result affected during the parcel retrieval is highly desirable to reduce possible injuries [44]. The incorporation of shielding frames or cage structures [79] is a trade-off between safety and weight increase that should rely on reasonable assumptions. For example, the simple carbon fiber front panel integrated in the FAMR shown in Fig. 3 serves to support the basket and at the same time protects the user from the pro-

[1] According to the handbook on "Best practice dropped object prevention".

pellers for a range of heading angles around ±30 degrees, taking into account that in normal operation, the aerial platform moves forwards when approaching the user. Also, if the user employs some kind of stick with a hook to retrieve the parcel instead of directly grasping it with his/her hands (see experiment in Sect. 6.4), safety can be significantly improved.

Multi-rotor crash may occur due to several reasons, considering as most common: impact or collision against an obstacle (including people, birds, traffic signals, other vehicles), battery discharge, electrical or electronic failure causing loss of thrust in one or several propellers, signal noise or interference in the onboard navigation sensors (GPS, IMU), or software bugs that may cause malfunctions. Besides previously mentioned risks, batteries should be also handled carefully since short-circuits or damages on their protecting case caused by strong impacts may result on fire. Particular works have been devoted to analyze the hazard and safety aspects of small drones [80], or the injuries falling drones may cause when impacting a human head [32].

4 System Modeling

4.1 Fully Actuated Multi-rotor Model

The dynamic model of the FAMR platform is derived using the Euler-Lagrange approach, following here the notation employed in [81] and [82]. The translational dynamics is expressed in the Earth frame $\{\mathbf{E}\} = \{\mathbf{X_E Y_E Z_E}\}$ and the rotational dynamics in the body frame $\{\mathbf{B}\} = \{\mathbf{X_B Y_B Z_B}\}$, as represented in Fig. 2. The FAMR state is defined by the vector $\boldsymbol{\xi} = \begin{bmatrix}\boldsymbol{p} & \boldsymbol{\eta}\end{bmatrix}^\top \in \mathbb{R}^6$, which includes the position $\boldsymbol{p} = [x,\ y,\ z] \in \mathbb{R}^3$ expressed in $\{\mathbf{E}\}$, and the Euler angles $\boldsymbol{\eta} = [\phi,\ \theta,\ \psi] \in \mathbb{R}^3$ of the attitude of the FAMR. In order to account for the parcel load/unload state, a binary variable δ_P is introduced, such that $\delta_P = 1$ when the parcel is dropped, and $\delta_P = 0$ when the basket is empty. This variable is used to update the mass/inertia parameters involved in the dynamic model of the platform, expressed in the usual matrix form as:

$$\begin{aligned}&\mathbf{M}(\boldsymbol{\xi}, \delta_P)\ddot{\boldsymbol{\xi}} + \mathbf{C}(\boldsymbol{\xi}, \dot{\boldsymbol{\xi}}, \delta_P)\dot{\boldsymbol{\xi}} + \mathbf{G}(\boldsymbol{\xi}, \delta_P)\\ &\quad = {}^{\mathbf{E}}\mathbf{R_B}\mathbf{F_C}(\omega_i) + \mathbf{F}_{PI} + \mathbf{F}_{ext}\end{aligned} \tag{1}$$

where $\mathbf{M} \in \mathbb{R}^{6\times6}$ is the inertia matrix, $\mathbf{C} \in \mathbb{R}^6$ represents the centrifugal and Coriolis terms, whereas $\mathbf{G} \in \mathbb{R}^6$ includes the gravitational forces. In addition, $\mathbf{F}_C = \begin{bmatrix}F_x & F_y & F_z & \tau_x & \tau_y & \tau_z\end{bmatrix}^\top \in \mathbb{R}^6$ includes the control forces and torques generated by the propellers, while $\mathbf{F}_{PI} \in \mathbb{R}^6$ includes the physical interaction forces and torques with the human/LiCAS. Finally, ${}^{\mathbf{E}}\mathbf{R_B} = [\mathbf{R_{EB}}\ \mathbf{0}_{3\times3};\ \mathbf{0}_{3\times3}\ \mathbf{I}_{3\times3}] \in \mathbb{R}^{6\times6}$ incorporates the rotation matrix $\mathbf{R_{EB}} \in \mathbb{R}^{3\times3}$ from $\mathbf{B}$ to $\mathbf{E}$, and $\mathbf{F}_{ext} \in \mathbb{R}^6$ represents the external forces and torques not modeled like aerodynamic effects.

The control forces and torques are related with the rotation velocity of each propeller using the mapping matrix $\boldsymbol{H}_{6\times6}$. For the FAMR, this matrix depends on the angles α and β, the length L from the center of gravity (CoG) of the platform to the motor, the drag coefficient C_D and the thrust coefficient C_T:

$$\mathbf{F_C}(\omega_i) = \begin{bmatrix}F_x\\F_y\\F_z\\\tau_x\\\tau_y\\\tau_z\end{bmatrix} = \underbrace{\begin{bmatrix}\boldsymbol{A_{3\times6}}C_T\\ \boldsymbol{B_{3\times6}}LC_T + \boldsymbol{C_{3\times6}}C_D\end{bmatrix}}_{\boldsymbol{H_{6\times6}}} \begin{bmatrix}\omega_1^2\\\omega_2^2\\\omega_3^2\\\omega_4^2\\\omega_5^2\\\omega_6^2\end{bmatrix} \tag{2}$$

where ω_i is the rotational speed of the motor i. The matrix $\boldsymbol{A}_{3\times6}$, $\boldsymbol{B}_{3\times6}$ and $\boldsymbol{C}_{3\times6}$ are shown in (3), (4) and (5), where c is cos, s is sin and A_i is the column i of $\boldsymbol{A}_{3\times6}$ (in the following $s\alpha$ and $c\alpha$ denote the sinus/cosine of α):

$$\boldsymbol{A}_{3\times6} = \begin{bmatrix}\frac{\sqrt{3}}{2}s\beta - \frac{s\alpha c\beta}{2} & s\alpha c\beta & -\frac{\sqrt{3}}{2}s\beta - \frac{s\alpha c\beta}{2} & \frac{\sqrt{3}}{2}s\beta - \frac{s\alpha c\beta}{2} & s\alpha c\beta & -\frac{\sqrt{3}}{2}s\beta - \frac{s\alpha c\beta}{2}\\ \frac{s\beta}{2} + \frac{\sqrt{3}}{2}s\alpha c\beta & -s\beta & \frac{s\beta}{2} + \frac{\sqrt{3}}{2}s\alpha c\beta & \frac{s\beta}{2} + \frac{\sqrt{3}}{2}s\alpha c\beta & -s\beta & \frac{s\beta}{2} - \frac{\sqrt{3}}{2}s\alpha c\beta\\ c\alpha c\beta & c\alpha c\beta & c\alpha c\beta & c\alpha c\beta & c\alpha c\beta & c\alpha c\beta\end{bmatrix} \tag{3}$$

$$\boldsymbol{B}_{3\times6} = \begin{bmatrix}\frac{c\alpha c\beta}{2} & c\alpha c\beta & \frac{c\alpha c\beta}{2} & -\frac{c\alpha c\beta}{2} & -c\alpha c\beta & -\frac{c\alpha c\beta}{2}\\ \frac{\sqrt{3}}{2}c\alpha s\beta & 0 & \frac{\sqrt{3}}{2}c\alpha s\beta & \frac{\sqrt{3}}{2}c\alpha s\beta & 0 & -\frac{\sqrt{3}}{2}c\alpha s\beta\\ s\alpha c\beta & -s\alpha c\beta & c\alpha c\beta & -s\alpha c\beta & c\alpha c\beta & -s\alpha c\beta\end{bmatrix} \tag{4}$$

$$\boldsymbol{C}_{3\times6} = \begin{bmatrix}-\mathrm{A}_1 & \mathrm{A}_2 & -\mathrm{A}_3 & \mathrm{A}_4 & -\mathrm{A}_5 & \mathrm{A}_6\end{bmatrix} \tag{5}$$

A more in detail derivation of these matrices can be found in [46]. Matrix **A** is part of the mixer matrix that is determined by the configuration of the rotors described at the end of Sect. 3.1, comprising a rotation sequence to change the direction of the thrust which allows to achieve the fully actuated configuration. In particular matrix **A** allows to obtain the forces on the XYZ axes from the angular velocity of the propellers. Matrix **B** is analogous to **A** but for the torques acting on the multi-rotor.

4.2 LiCAS Kinematics and Dynamics

The LiCAS dual arm manipulator implements the kinematics depicted in Fig. 4 with four positioning joints, three at the shoulder and the elbow. Wrist orientation joint are not implemented since these are not necessary for the intended operation and due to the convenience to reduce the mass and inertia of the arms. Denoting by q_j^i the rotation angle of the j-th joint of the i-th arm ($i = \{1, 2\}$ for the left and right arms, respectively), the rotation angles of the arms are:

- Shoulder flexion/extension, q_1^i.
- Shoulder adduction/abduction, q_2^i.
- Lateral/medial rotation, q_3^i.
- Elbow flexion/extension, q_4^i.

The lengths of the two main links of the arms, upper arm and forearm, are denoted by L_1 and L_2, respectively, whereas D will denote the separation distance between the arms. The dual arm base frame $\{\mathbf{0}\}$ is attached at the midpoint of the baseline of the shoulder flexion/extension joint, with the $\mathbf{X_0}$ axis pointing forwards, and the $\mathbf{Z_0}$ axis pointing upwards, as represented in Fig. 2. Analytical resolution of this kinematic configuration is detailed in [51].

The dynamics of the LiCAS manipulator is obtained following the Euler-Lagrange formulation, adopting the flexible joint model [83] to account for the spring-lever transmission mechanism introduced between the servo actuators and the links (see Fig. 5). Since both arms are kinematically and mechanically identical, and are rigidly attached to the ground through the shoulder structure, there is no dynamic coupling between them except for the external wrenches exerted in closed kinematic chain, for example when the right arm arm is holding the FAMR while the left arm drops the parcel on the basket (see Sect. 6.3). Therefore, the equations of motion in joint space can be expressed for each arm as:

$$\mathbf{M}(\mathbf{q}^i)\ddot{\mathbf{q}}^i + \mathbf{C}(\mathbf{q}^i, \dot{\mathbf{q}}^i)\dot{\mathbf{q}}^i + G(\mathbf{q}^i) = \boldsymbol{\tau}^i + \boldsymbol{\tau}^i_{ext} \tag{6}$$

$$\mathbf{B}(\boldsymbol{\theta}^i)\ddot{\boldsymbol{\theta}}^i + \boldsymbol{\tau}^i = \boldsymbol{\tau}^i_s - \boldsymbol{\tau}^i_f \tag{7}$$

$$\boldsymbol{\tau}^i = \mathbf{K}^i(\boldsymbol{\theta}^i - \mathbf{q}^i) + \mathbf{D}(\dot{\boldsymbol{\theta}}^i - \dot{\boldsymbol{q}}^i) \tag{8}$$

Here $\mathbf{M}$ and $\mathbf{B} \in \mathbb{R}^{4\times4}$ are the inertia matrices of the output links and the servo shafts, respectively (the terms in $\mathbf{B}$ are much lower than in $\mathbf{M}$), $\mathbf{C} \in \mathbb{R}^{4\times4}$ contains the centrifugal and Coriolis terms, $\mathbf{G} \in \mathbb{R}^4$ are the gravity torques, whereas $\tau_s^i \in \mathbb{R}^4$ is the torque vector of the servo actuators, $\tau^i \in \mathbb{R}^4$ is the torque transmitted by the spring-lever mechanism, and $\tau_{ext}^i \in \mathbb{R}^4$ are the external torques acting on the arm. Two kind of external wrenches are considered here: (1) those exerted by the basket of the FAMR while this is hovering during the parcel load operation, (2) the forces exerted by each of the arms into the other when forming a close kinematic chain during parcel load.

The spring-lever transmission is assimilated to a torsion spring-damper characterized by its stiffness k_j^i and damping d_j^i, so the corresponding joint stiffness and damping matrices are $\mathbf{K}^i = diag(\{k_j^i\})$ and $\mathbf{D}^i = diag(\{d_j^i\})$. Again, since both arms are identical, it is possible to assume that $k_j^1 = k_j^2 \; \forall j$. The equivalent joint stiffness of the spring-lever transmission is obtained from the compression spring stiffness $K_{S,j}^i$ and the lever length L_s as $k_j^i = K_{S,j}^i L_S^2$, whereas the joint damping should be experimentally determined as in [53].

The joint deflection angle $\Delta\theta_j^i$ caused by the compression of the springs due to any endogenous or exogenous force is defined as the difference between the servo shaft and the angular position of the corresponding output link, that is, $\Delta\theta_j^i = \theta_j^i - q_j^i$. Analogously, the Cartesian deflection is defined as the position deviation of the end effector in the compliant arm with respect to the equivalent stiff-joint arm [19, 53]:

$$\boldsymbol{\Delta}\mathbf{l}^i = \mathbf{FK}(\boldsymbol{\theta}^i) - \mathbf{FK}(\mathbf{q}^i) \tag{9}$$

For small deflection angles, the Cartesian deflection can be obtained from the manipulator Jacobian and the deflection vector as:

$$\boldsymbol{\Delta}\mathbf{l}^i = \mathbf{J}(\boldsymbol{\theta}^i)\boldsymbol{\Delta}\boldsymbol{\theta}^i \tag{10}$$

The dynamics of the compliant manipulator can therefore be expressed in the Cartesian space as follows [53]:

$$\mathbf{M}_C\ddot{\boldsymbol{\Delta}}\mathbf{l}^i + \mathbf{D}_C\dot{\boldsymbol{\Delta}}\mathbf{l}^i + \mathbf{K}_C(\boldsymbol{\Delta}\mathbf{l}^i - \boldsymbol{\Delta}\mathbf{l}_0^i) + \boldsymbol{\Delta}\mathbf{l}_G^i = \mathbf{F}^i + \mathbf{F}_{ext}^i \tag{11}$$

where $\mathbf{K}_C \in \mathbb{R}^{3\times3}$ and $\mathbf{D}_C \in \mathbb{R}^{3\times3}$ are the Cartesian stiffness and damping matrices [53], $\boldsymbol{\Delta}\mathbf{l}_0^i$ is the zero deflection reference position, $\mathbf{F}^i$ are the forces generated by the manipulator, whereas $\mathbf{F}_{ext}^i$ are the external forces at the end effector, exerted either by the FAMR basket or by the other arm.

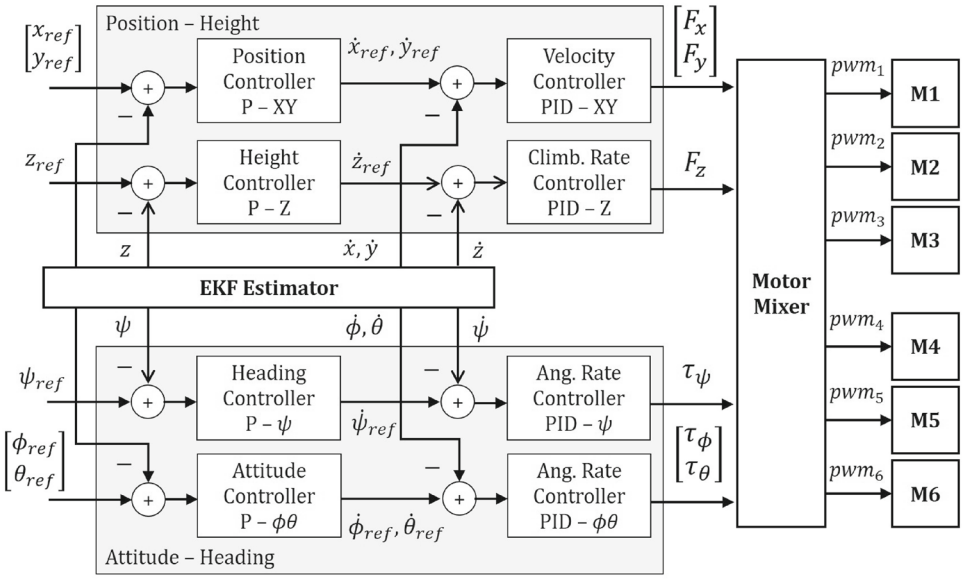

Fig. 7 FAMR position-attitude cascade controller implemented by flight controller

5 Control Framework

5.1 FAMR Cascade Controller

Given the diversity of position and attitude controllers that can be found in the literature [64], a cascade control scheme is adopted in this work for the FAMR due to three main reasons: (1) this control architecture is implemented by most standard autopilots due to their reliability and robustness to perturbations (experimentally evaluated in Sect. 6.2), reducing consequently the development and validation time towards system implementation, (2) the interpretation and tuning procedure of the controller parameters is more intuitive, and (3) it can be used as baseline controller for further improvement and comparison with other control schemes. In particular, next subsection addresses the incorporation of an admittance control layer [17] based on a deflection interpretation of the position/attitude control errors to allow the user guiding the platform by applying contact wrenches [51].

Unlike the typical implementation in co-planar multi-rotors, in which the position control is achieved through the attitude control due to the under-actuated dynamics, the fully actuated multi-rotor allows to decouple the attitude and position control, as depicted in Fig. 7. A Proportional (P) controller takes as input position/attitude references and gives as output the corresponding speed references, taken as input by a Proportional-Integral-Derivative (PID) controller that computes the required wrenches converted into a PWM (pulse width modulation) signal through the Motor Mixer.

Particularizing for the X-axis position control:

$$\dot{x}_{ref} = K^{p}_{Px}(x_{ref} - x) \tag{12}$$

$$F_x = K^{v}_{Px}\dot{x}_e + K^{v}_{Ix}\int \dot{x}_e\, dt + K^{v}_{Dx}\ddot{x}_e \tag{13}$$

where $\dot{x}_e = \dot{x}_{ref} - \dot{x}$ is the X-axis velocity error, K^{p}_{Px} is the X-axis proportional gain of the position controller, and K^{v}_{Px}, K^{v}_{Ix}, and K^{v}_{Dx} are the proportional, integral, and derivative gains of the X-axis velocity controller acting over the corresponding velocity error $\dot{x}_e$. The integral term is typically saturated to a maximum value to prevent wind-up effect. An Extended Kalman Filter (EKF) is implemented to obtain position, velocity, and acceleration estimates from the fusion of the on-board and off-board sensors (accelerometer, gyroscope, magnetometer, visual position sensors, and others). The controller is analogous for the other axes, as well as for the attitude control. Note that the gain K^{v}_{Px} relates the force exerted by the FAMR to velocity errors, so it can be interpreted as a damping factor, whereas the term $K^{p}_{Px}K^{v}_{Px}$ corresponds to the stiffness factor that relates the position deviation with the exerted force.

5.2 FAMR Equivalent Compliant Model

The ability of the FAMR to decouple the position and attitude control, represented in Fig. 7, along with the assimilation of the controlled platform to a second order dynamic system characterized by its mass/inertia and an equivalent stiffness/damping coefficients mentioned above, allow the application of control methods from series elastic actuators [84], developed also in our previous works for compliant aerial manipulators [51, 53]. The key concept is the interpretation of the FAMR position/attitude errors as Cartesian/angular deflection values, defined as the difference between the reference (considered as "stiff" value) and current pose. Denoting by $\mathbf{F}_{ext} = [F^{ext}_x, F^{ext}_y, F^{ext}_z]^\top$ the external forces that the human user may exert at the bas-

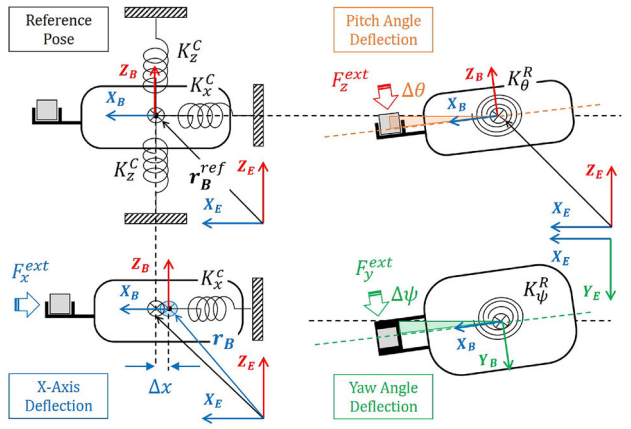

Fig. 8 Equivalent compliant model of the fully actuated multi-rotor, where the position/attitude control errors are interpreted as deflection values

ket, it is assumed that the deflection will only occur in the X-axis, and in the pitch and yaw angles, as depicted in Fig. 8.

For relatively small forces and position/attitude deviations (in the range of 0.1 m / 10 degrees), it is possible to assimilate the position-controlled FAMR to an equivalent linear/torsion spring system such that:

$$F_x^{ext} = K_x^C(x_{ref} - x) = K_x^C \Delta x \tag{14}$$
$$F_y^{ext} = K_\psi^R(\psi_{ref} - \psi) = K_\psi^R \Delta\psi \tag{15}$$
$$F_z^{ext} = K_\theta^R(\theta_{ref} - \theta) = K_\theta^R \Delta\theta \tag{16}$$

where K_x^C, K_ψ^R, and K_θ^R are the equivalent Cartesian and rotational stiffness constants for the X-axis and the pitch-yaw angles, respectively, whose value is mainly determined by the proportional gains of the position-velocity cascade controller and on the distance L_b from the basket to the center of mass of the platform, whereas Δx, $\Delta\theta$, and $\Delta\psi$ are the corresponding deflection values. Identification methods based on impulsive response or quasi-static force–deflection characterization [53] can be applied to estimate the value of these parameters. Section 6.2 will present experimental results with the response of the FAMR to impulsive and pushing forces exerted in the X-axis and in pitch and yaw angles.

5.3 FAMR Control with Physical Human Interaction

In order to allow the human user to interact physically with the FAMR through the basket, for example for adjusting the height of the platform to retrieve the parcel more comfortably, as illustrated in Fig. 9, a modified version of the zero-deflection controller developed for compliant arms in [51] is applied here, inspired also in the admittance controller for quadrotors presented in [17].

The interaction model with the human user involves the application of the three type of forces on the basket as identified in Figs. 8 and 9:

1. Pushing/pulling forces along the Z-axis (F_z^{ext}) that tend to cause tilting deviations in pitch ($\Delta\theta$) while maintaining fixed the position of its center of mass.
2. Lateral forces (F_y^{ext}) that tend to induce deviations in the yaw angle of the platform ($\Delta\psi$) while maintaining fixed the position of its center of mass.
3. Pushing forces along the X-axis (F_x^{ext}) that cause linear displacements (Δx) to move away the multi-rotor while maintaining its attitude constant.

These forces may be impulsive or assimilated to certain patterns (step, stair, or smooth variations), assuming in any case that the user applies them on the basket with his/her hand or through a device like the stick with hook employed in the tests. Sections 6.2 and 6.4 evaluate experimentally the response of the multi-rotor to these kind of interactions. The relationship between force exerted by the user and the deflection inducted on the platform is given by Eqs. (14)–(16). Note that, since the FAMR decouples attitude from position control thanks to the convenient arrangement of the propellers described in Sect. 3.1, the forces exerted by the user at the basket on the YZ-axes is transformed into a torque at the CoM of the multi-rotor.

The natural way for the user to adjust the position of the aerial platform for retrieving more comfortably the parcel would be grabbing the basket and pulling it up/down, left/right, or forwards/backwards, which involves the application of the external force $\boldsymbol{F}_{ext}$ depicted in Figs. 8 and 9. Therefore, the desired behaviour for the FAMR when interacting with the user to be implemented by the admittance controller on top of the position controller is as follows:

- Reduce/increase the reference height of the platform (z_{ref}) when the user exerts a pushing/pulling force against the basket (F_z^{ext}) causing a deflection in pitch ($\Delta\theta$).
- Move laterally the platform (y_{ref}) when the user exerts a yaw moment ($\Delta\psi$) due to a lateral force (F_y^{ext}).
- Move the platform forwards/backwards (x_{ref}) when the user exerts a pushing force along the X-axis.

These corrections on the nominal position of the multi-rotor (x_{ref}, y_{ref}, z_{ref}) with respect to the reference frame of the window (see Fig. 2), are intended to correct the positioning of the FAMR in the most convenient way for the user according to the particular type of window and the way he/she extends his/her arms through it.

As described in [17], the desired guiding effect can be achieved implementing an admittance controller that modi-

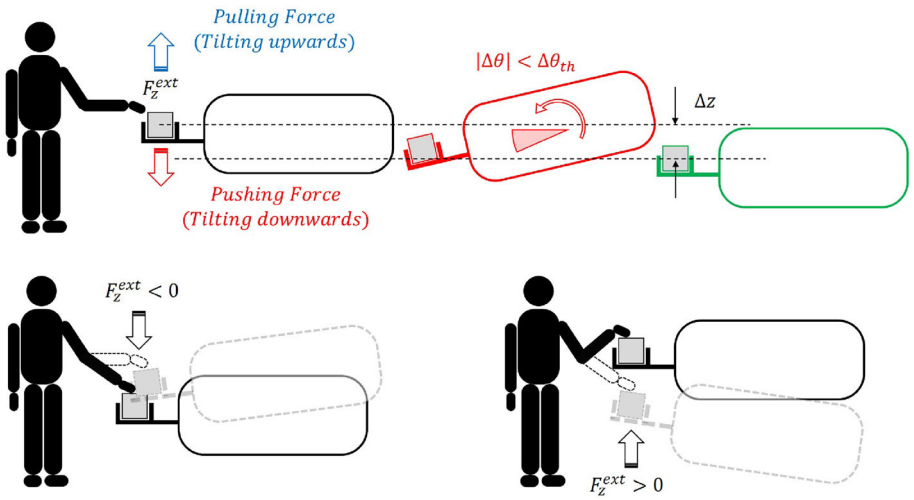

Fig. 9 Desired altitude control behaviour when the user pushes/pulls the payload along the Z-axis. An altitude correction Δz is introduced when the pitch angle exceeds the threshold ($|\Delta\theta| > \Delta\theta_{th}$) to prevent excessive tilting

fies the reference position of the FAMR platform in response to the forces exerted by the human user, imposing zero stiffness and considering only a damping factor. Similarly to the zero-deflection controller for the flexible joint manipulator in [51], the Cartesian and angular deflection of the platform can be used to estimate the external forces from the model given by Eqs. (14)–(16). The proposed control scheme is depicted in Fig. 10. Particularizing for the desired pitch-height interaction represented in Fig. 9, the altitude reference is computed as:

$$z_{ref} = z^0_{ref} + \int_0^t S_z \zeta(\Delta\theta, \Delta\theta_{th})\, dT \tag{17}$$

where z^0_{ref} is the nominal height reference, S_z is the Z-axis speed scaling factor, $\Delta\theta_{th} > 0$ is the pitch angle deflection threshold, and $\zeta(\cdot,\cdot) : \mathbb{R}\times\mathbb{R} \to \mathbb{R}$ is the dead-zone function defined as follows:

$$\zeta(\Delta\theta, \Delta\theta_{th}) = \begin{cases} \Delta\theta - \Delta\theta_{th} & \text{if } \Delta\theta > \Delta\theta_{th} \\ \Delta\theta + \Delta\theta_{th} & \text{if } \Delta\theta < -\Delta\theta_{th} \\ 0 & \text{in other case} \end{cases} \tag{18}$$

The platform will increase/decrease the height reference as long as the user applies the force, corresponding to the integral term in Eq. (17). In order to reject the effect of small attitude control errors or the noise in the measured pitch angle, only deflections above the threshold $\Delta\theta_{th}$ are considered as actions from the user, which motivates the introduction of Equation (18). The dead-zone function prevents integral drift due to measurement noise or small control errors, which determine the lower bound for the deflection threshold. Note that the units of the scaling factor S_z are m/(s rad), since the height ascending/descending rate is proportional to the pitch deflection angle. The method is the analogous for the yaw angle and the X-axis deflection, with the corresponding scaling factors and threshold values.

Table 3 Cascade controller parameters of the FAMR

Controller	Action	P	I	D
XY position	Distance to speed	1.0	–	–
XY velocity	Velocity to accel	2.0	0.2	1.2
XY velocity	Integral limit	–	–	25
Stabilize (attitude)	Roll-Pitch angles	4.5	–	–
Stabilize (attitude)	Yaw angle	1.0	–	–
Angular rate	Roll-pitch angles	0.25	0.35	0.004
Angular rate	Yaw angle	0.7	0.02	0
Altitude hold	Alt. to Climb rate	1.0	–	–
Throttle eate	Climb rate to accel	1.0	–	–

It is necessary to remark that the capacity of the multi-rotor to counteract the forces exerted by the user is limited by the maximum thrust of the propellers (multi-rotor hover is typically done at 50–60% of thrust to avoid actuators saturation). The compliant behaviour provided by the admittance controller allows to alleviate the effort supported during the interaction by accommodating the position of the platform, taking also into account that the ability of the human user to exert contact forces is limited by the reach of his/her arm.

6 Experimental Results

The results presented here were obtained with the cascade controller described in Sect. 5.1, flying the aerial platform in position mode. The controller parameters were tuned through the Mission Planner interface of the ArduPilot firmware, using the values indicated in Table 3.

The angular rate and attitude controllers were firstly tuned by an skilled human pilot, whereas the velocity and posi-

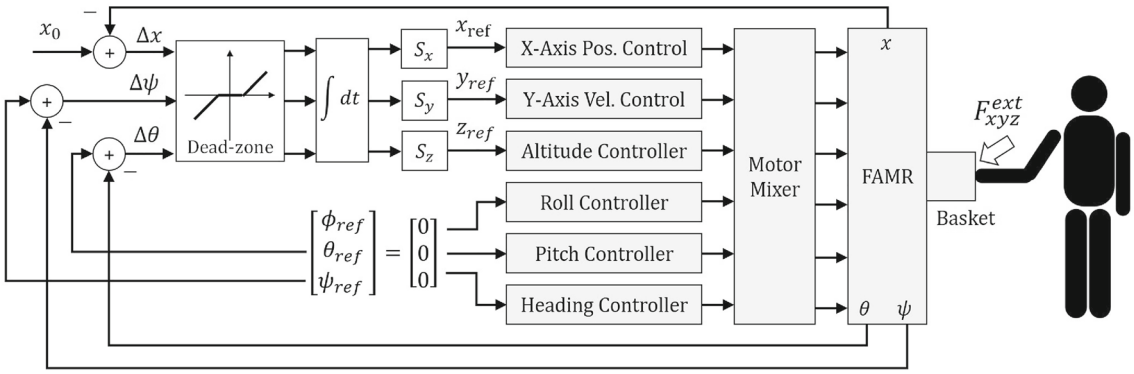

Fig. 10 Compliant human–FAMR interaction controller based on Cartesian and angular deflection. Position references are updated integrating the deflection signals, applying previously a dead zone to reject sensors noise and small control errors, so only the external forces applied by the user on the basket account for accommodating the position of the FAMR

tion controllers were later tuned based on the experimental identification of the overshoot and convergence time of the position controller to external perturbations exerted by the human user.

The experiments presented in Sect. 6.1 and 6.2, both involving close proximity between the human user and the aerial platform while flying, were carried out by researchers with significant experience in aerial robotics. In case these experiments are reproduced, it is strongly recommended to use appropriate equipment like protection gloves and glasses for safety reasons, and proceed with extra caution when approaching and interacting with the aerial platform. The use of a stick with a hook for interacting with the basked also contributes to improve safety by increasing the separation distance.

The datasets generated during and/or analysed during the current study are available from the corresponding author on reasonable request.

6.1 Parcel Load/Unload

The goal of this identification experiment is to evaluate the behaviour of the FAMR cascade controller when parcels of different weight are loaded/unloaded into the basket, as well as to obtain an estimation of the expected position deviation in order to account for the possible collision of the aerial platform with the manipulator or the user when these are in front of it during the operation. The execution of the experiment is depicted in Fig. 11. A human user drops/retrieves the parcel at intervals of 30 s while the aerial platform is hovering at fixed position at 1.2 m height and zero attitude reference. Three payloads are applied in three consecutive load/unload operations: 60, 90, and 120 grams, corresponding to a moment of 0.3, 0.45, and 0.6 Nm exerted in the pitch angle due to gravity (the basket is located at 0.5 m from the platform CoM). The evolution of the FAMR position displacement with respect to its reference position is depicted in Fig. 12, comparing in more detail the X-axis and pitch angle deviation of the platform in Fig. 13. As it can be seen, the effect of loading/unloading the parcel on the basket can be assimilated to an impulsive moment exerted in the pitch angle causing a consequent position deviation compensated by the cascade controller. The maximum X axis position displacement for the three masses are 0.5, 0.7, and 0.85 m, respectively.

The analysis and comparison of the data allows to derive the following remarks:

- The position and attitude deviations of the FAMR show the typical second order behaviour characterized by a certain stiffness and damping, which validates the equivalent compliant model described in Sect. 5.2.
- Parcel load causes a significant forward displacement on the aerial platform, along the $\mathbf{X_B}$ aixs, which could lead to a collision of the platform against the wall or the human user. This motivates the use of the right arm of the LiCAS manipulator to hold the platform during the load operation (see Sect. 6.3).
- Parcel unload causes a backward displacement on the aerial platform, in this case, a convenient reaction for the aerial delivery operation since this does not compromise safety as long as the platform has enough space behind.
- The parcel load/unload event can be easily detected by defining a threshold in the pitch angle (around $\pm 5\ deg$) and monitoring the X-axis displacement in order to distinguish this from other intentional interactions from the human user (see Sect. 6.2).
- The variation of the FAMR altitude is much lower compared to the displacement along the $\mathbf{X_B}$ axis. Also, the lateral displacement is lower, but there is a certain coupling.
- The reaction time of the aerial platform to these position deviations due to mass unbalance is around 2 s, which

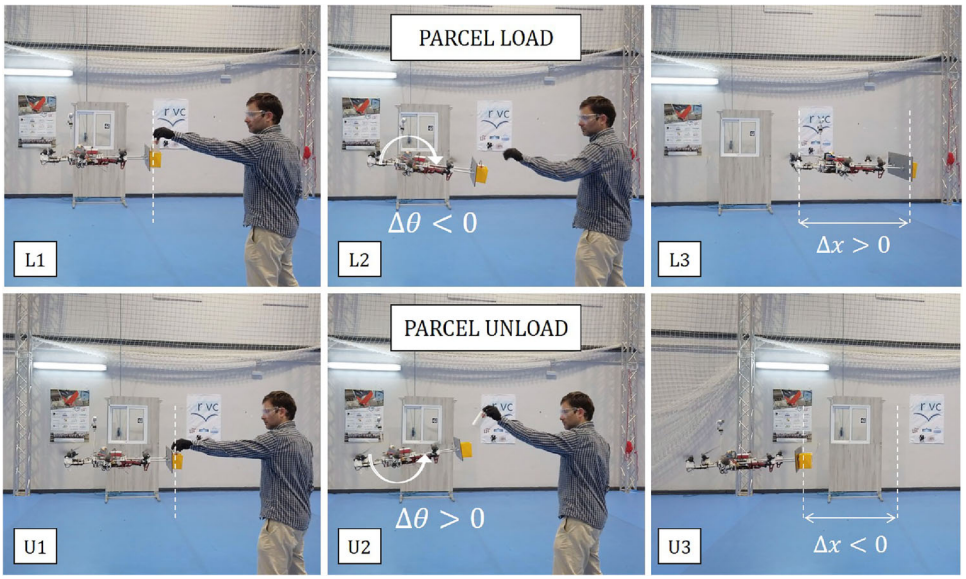

Fig. 11 Image sequence showing the FAMR deviation in pitch and X-axis during parcel load and unload. User drops/retrieves the parcel from the basket (L1/U1), the platform suffers an instantaneous deviation in the pitch angle (L2/U2) and a consequent deviation along the $\mathbf{X_B}$ axis (L3/U3)

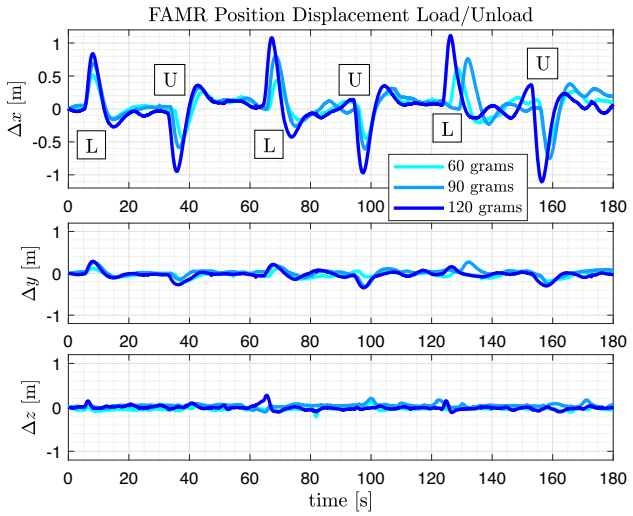

Fig. 12 Position displacement of the FAMR when the parcel is loaded (L) and unloaded (U) on the basket, considering three payloads: 60, 90, 120 gs

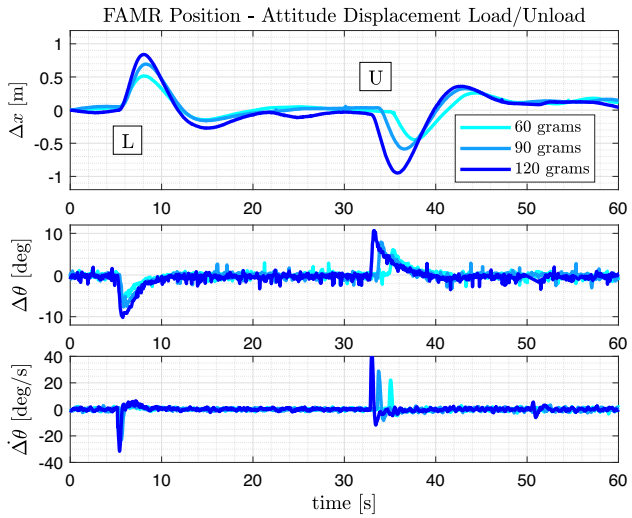

Fig. 13 Detailed view of the X-axis position and pitch angle deviation of the FAMR for the three payload masses

determines the required agility of the human user or the robotic manipulator to drop or retrieve the parcel, unless the delivery basket is grabbed to prevent this inconvenience.

It is necessary to remark that during the experiments, the FAMR platform is commanded to maintain a zero attitude reference, and therefore, the actuation of the position controller is limited by the horizontal force that can be exerted by the tilted propellers, which is limited to 4 N approximately. The dynamic response of the FAMR in terms of overshoot and convergence time to the position reference after the perturbation associated to the parcel load/unload event occurs, could be improved by removing the zero attitude constraint and allowing the platform to tilt to increase the magnitude of the horizontal forces that the platform can generate to counteract the sudden mass unbalance. This allows to implement schemes like geometric $L1$ adaptive control [85], adaptive non-singular fast terminal sliding mode control [86], adaptive backstepping [87], or hybrid robust adaptive control [88]. Note however that, in the close interaction with the human user, it is still preferable that the multi-rotor controller is slightly "slow" to prevent that fast reactions from the position controller scare the user or make the handover operation more uncomfortable.

Since previous experiments were conducted with the same battery (LiPo 4 S, 4.500 mAh, 0.5 kg weight), it is also interesting to compare the discharge rate and power consumption,

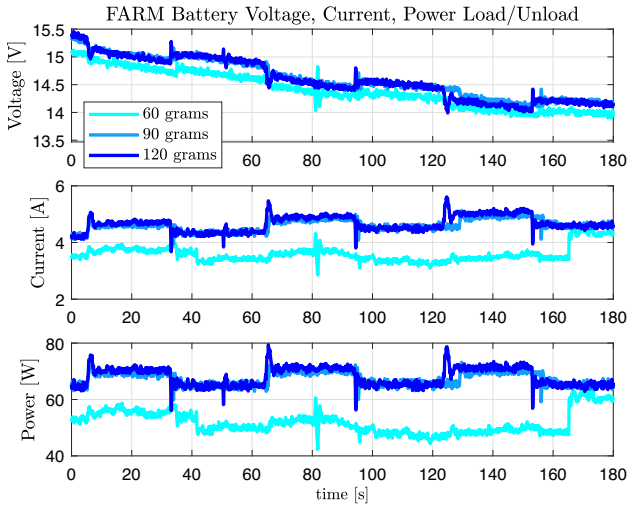

Fig. 14 Battery discharge rate for the three payload masses. Battery voltage (up), current (middle), and power (down)

represented in Fig. 14. Note that for the 60 grams case the initial voltage of the battery is 0.5 V lower than in the other two cases, and the current consumption is also 0.5 A below.

6.2 Impulsive and Pushing Forces Exerted by Human User

The purpose of these experiments is twofold. On the one hand, demonstrating the stability and reliability of the attitude-position cascade control scheme described in Sect. 5.1 to impulsive and pushing forces exerted on the basket, taking into account that safety is an essential requirement in this application. Since the human user is intended to interact with the FAMR during the parcel load/unload, it is necessary to evaluate the behaviour of the platform to a range of "reasonable" perturbations that the human might exert by pushing, pulling or grabbing the platform by hand, as depicted in Fig. 15 (see video attachment). The response of the FAMR to this set of randomly exerted perturbations is represented in Fig. 16, including the case in which the user grabs the basket and disturbs the platform in roll, pitch and yaw.

On the other hand, these experiments evidence the position-attitude decoupled dynamics and control of the fully actuated configuration, and the obtained results can be used to identify the equivalent spring-damper parameters that relate the exerted force with the attitude and position deviations, assimilating the controlled platform to an passive mechanical system with second order dynamics. During the experiment, the FAMR is commanded to hover at a fixed position with zero attitude reference while the human user exerts pushing forces at the basket, causing: (1) X-axis position deviations, (2) tilting moments in pitch angle, and (3) yaw rotations. In order to measure the magnitude of the forces applied in the basket, a calibrated compliant force sensor consisting of a HGSI LPPS-SL-025 linear potentiometer (25 mm stroke) and a low stiffness compression spring is attached at the tip of a rod used to exert the forces, reading the measurements through an microcontroller board connected to the Ground Control Station (GCS) laptop. The response of the FAMR position and attitude controllers to these impulsive and sus-

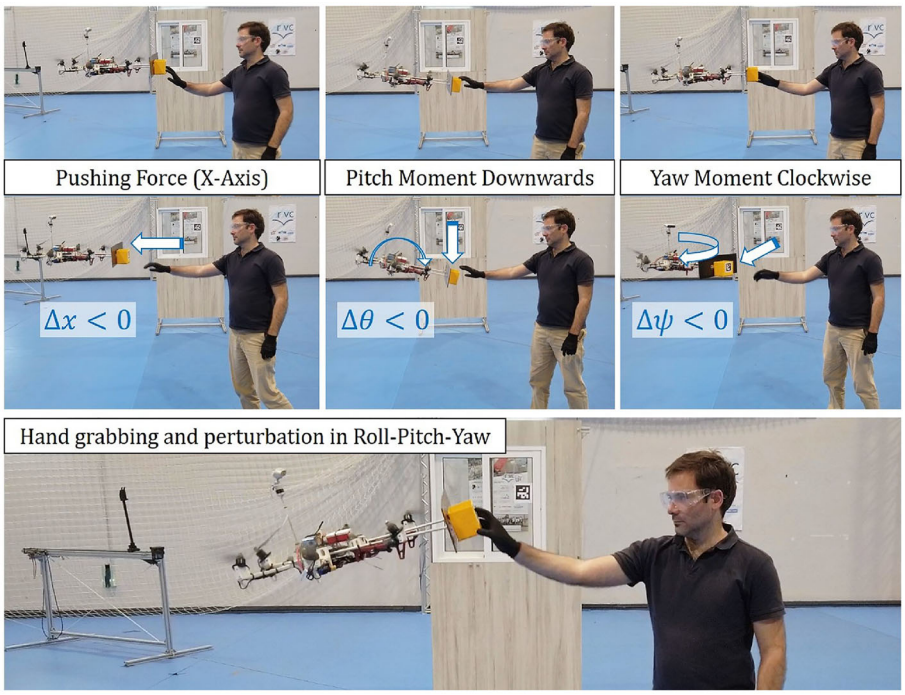

Fig. 15 Human user exerting different impulsive and pushing forces against the basket of the FAMR. Particular care must be taken when replicating this experiment since instability of multi-rotor controller due to excessive perturbations may cause injuries on the user in case of impact of propellers

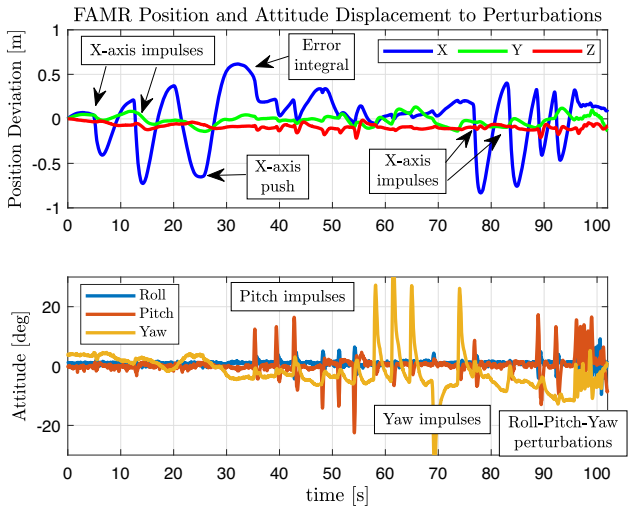

Fig. 16 FAMR position and attitude deviations to significant perturbations exerted by the human user by hand over the basket: X-axis impulses and pushing forces (0–30 s, and 75–90 s), pitch and yaw impulses (35–75 s), and roll-pitch-yaw perturbation while grabbing the basket (90–100 s)

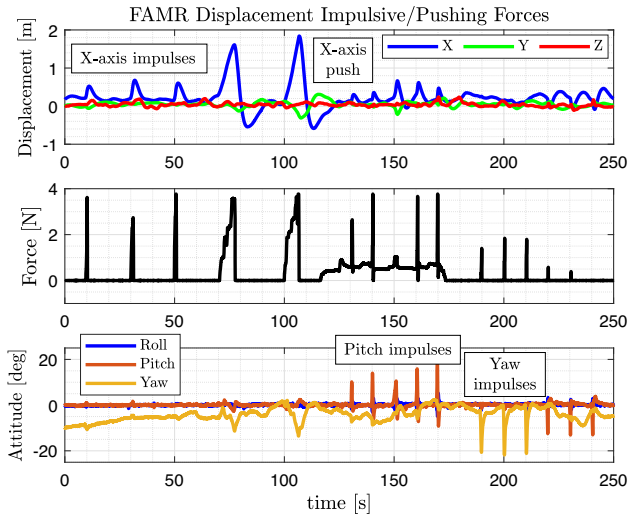

Fig. 17 FAMR position and attitude deviations to pushing forces and moments exerted through a compliant force sensor along the X-axis, the pitch and yaw angles. The contact occurs at the basket located at 0.5 m from the platform center of mass

tained forces is represented in Fig. 17. The force ramp signal manually applied by the human user at $t = 70$ and $t = 100$ s reveals that the equivalent X-axis stiffness of the position controller is 2 N/m, approximately.

During the realization of the tests, it was found that the cascade controller implemented in the FAMR remained stable without raising any unstable behaviour. Even in the most risky situation in which the user exerts a pitch moment downwards (see Fig. 15 in the middle), the platform was able to maintain the position and attitude control thanks to the fully actuated feature. The carbon fiber protection panel that separates the propellers from the basket contributes to enhance the feeling of safety of the user compared to the case in which the rotors are not covered. The main inconvenience observed was the relatively low convergence time and significant overshoot when peak or sustained forces are exerted on the X-axis due to the limited ability of the FAMR to generate horizontal forces and because errors accumulated in intervals of few seconds tend to saturate the integral action. Anyways, it is preferable that the convergence time in the position control is relatively slow so the user feels comfortable and safe when the platform is moving closely.

6.3 Parcel Load on Flight with LiCAS

This experiment is intended to demonstrate the possibility to conduct the parcel load on flight relying on the compliant bimanual manipulation capabilities of the LiCAS dual arm presented in Sect. 3.2. The operation is depicted in Fig. 18. As analysed in Sect. 6.1, the FAMR experiences a significant pitch and position deviation in the forward direction when the parcel is dropped into the basket due to the sudden mass unbalance (see Fig. 12). In order to prevent the collision of the FAMR with the LiCAS due to this effect, and taking benefit of the human-like manipulation capabilities of the arms, the adopted solution consisted of holding the base of the basket of the FAMR with the right arm while the parcel is loaded with the left arm, exploiting the mechanical joint compliance of the LiCAS to overcome the interaction wrenches due to the pose deviations of the FAMR. The evolution of the tool center point (TCP) position of both arms, the joint variables, and the position and attitude deviation of the FAMR platform with respect to the hovering position are depicted in Fig. 19. For simplicity in the realization of the experiments, the LiCAS is teleoperated using another LiCAS with identical kinematic configuration in leader-follower configuration [89]. The operation starts once the FAMR is hovering in front of the LiCAS, such that the basket is at a relative XYZ position of $[0.3, -0.15, -0.25]$ m with respect to the arms frame $\{\mathbf{0}\}$, corresponding to the L-pose of the right arm. The right forearm is lifted until the two electromagnets placed at the end effector are in contact with the metallic base of the basket (phase 1 in Fig. 19) in order to provide a certain grip. Then, the left arm, which is initially holding the parcel by the handle with a hook-like gripper using the gravity effect, is moved until the XY components of both arms are aligned (phase 2). Once the parcel is dropped in the basket and the left arm is released, this goes back to the rest position (phase 3) and then the right arm pushes the FAMR 10 cm backwards along the X-axis so the FAMR position/attitude controllers can compensate the mass unbalance due to the load without colliding with the arms.

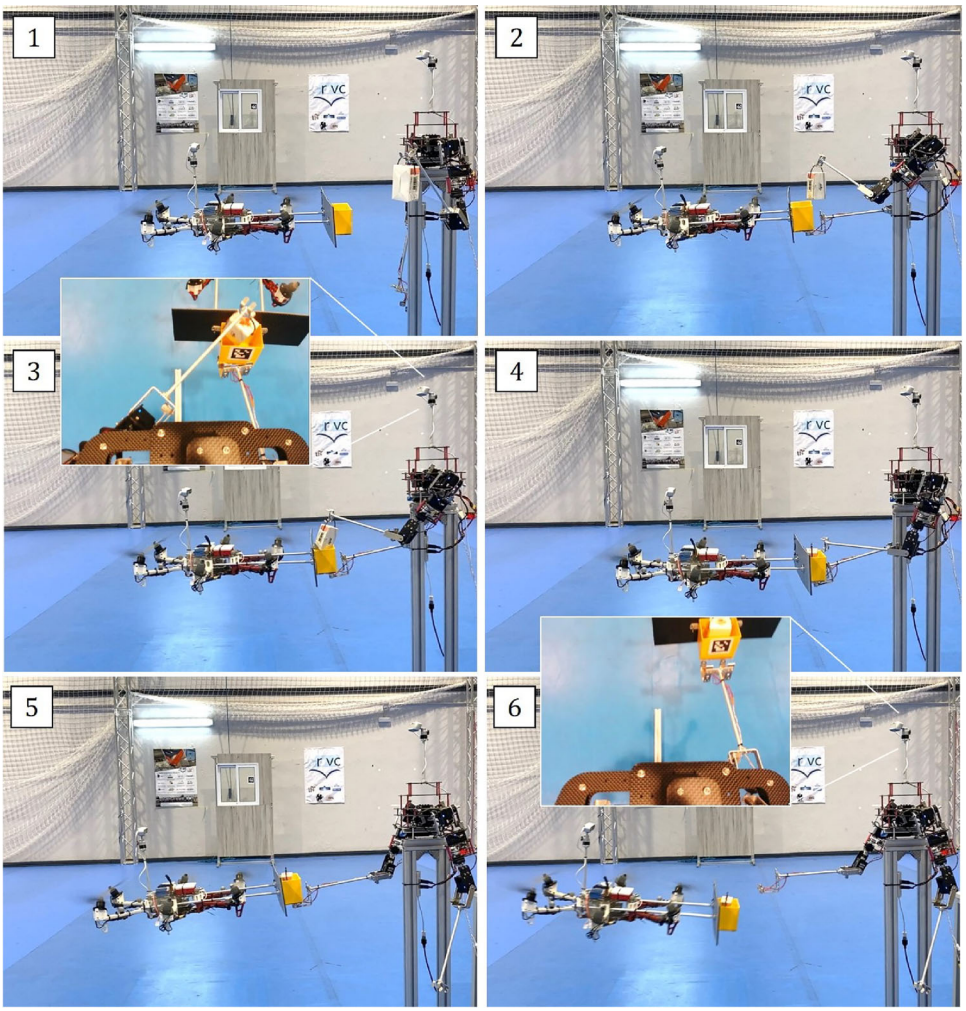

Fig. 18 Sequence of images showing how the LiCAS manipulator drops the parcel on the basket while the right arm holds its base to prevent the FAMR position and attitude displacement causing a collision with the arms

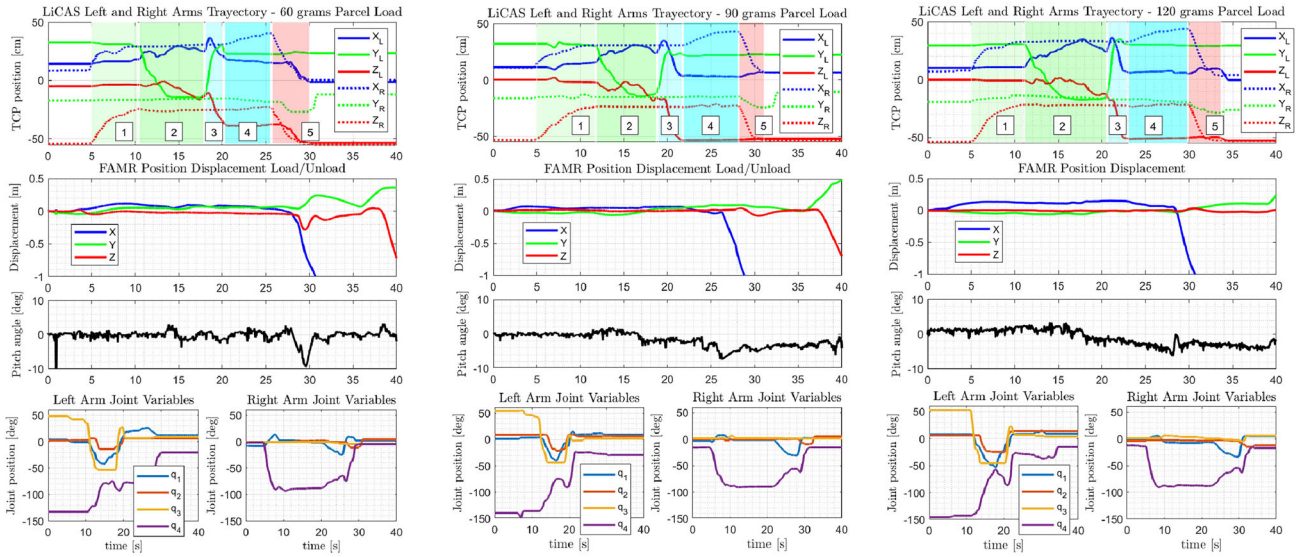

Fig. 19 Tool center point (TCP) position of the LiCAS left and right arms (up), FAMR position and pitch angle deviation w.r.t. the hovering position (middle), and LiCAS joint angular position (down) during the parcel load operation for the 60 gs (left), 90 gs (middle), and 120 gs (right) payloads. The right arm (dashed line) is used to hold the base of the basket (phases 1–2), whereas the left arm (solid line) drops the parcel on the basket (phase 3–4)

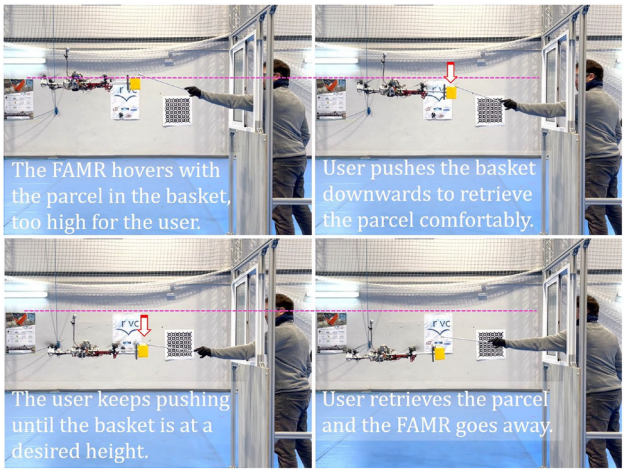

Fig. 20 Sequence of images illustrating the delivery operation with user interaction for adjusting the height by applying a downwards pushing force with the stick

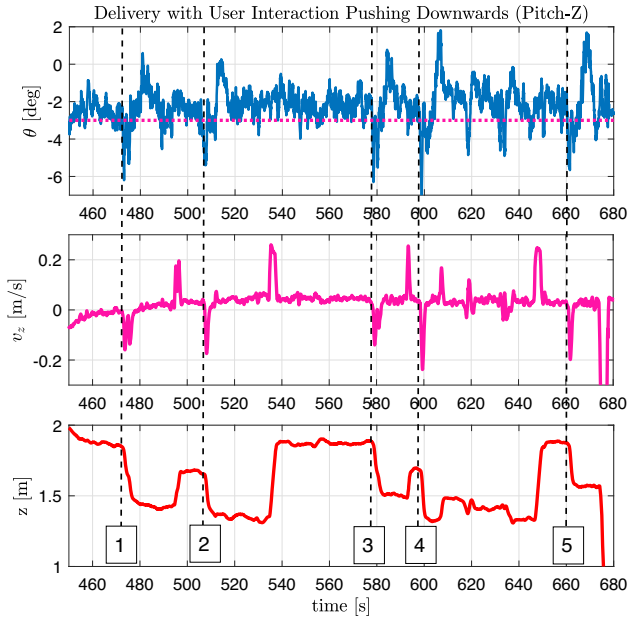

Fig. 21 Evolution of the FAMR pitch, Z-axis speed and position when the human user exerts a pushing force downwards with the stick so he/she can retrieve the parcel more comfortably. Five consecutive interactions were tested

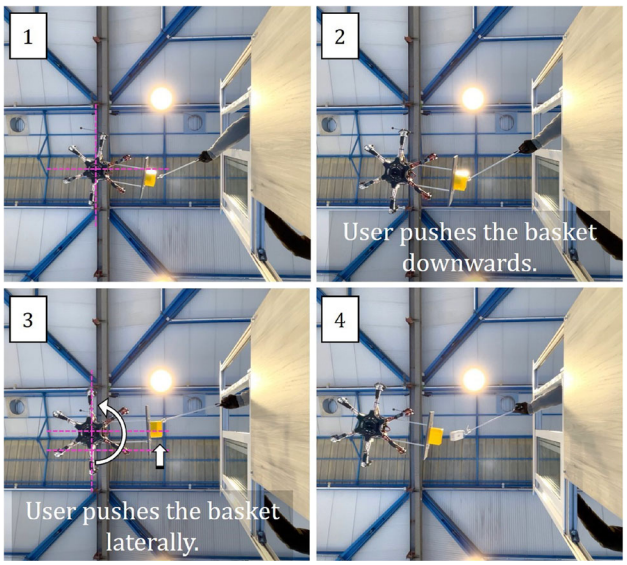

Fig. 22 Sequence of low angle images illustrating how the FAMR adapts its height and lateral position according to the interaction forces exerted by the user through the window in order to bring the parcel to a comfortable position for retrieval

6.4 Multi-rotor Interaction Control Experiments

The experimental results presented here evaluate the response of the FAMR compliant interaction controller described in Sect. 5.3 to the pushing/pulling forces exerted by the user when retrieving the parcel from the basket. Two use cases are considered. On the one hand, Figs. 20 and 21 represent the case in which the user is exerting a certain pushing force downwards against the basket, causing an instantaneous pitch moment on the multi-rotor that is supported by the attitude controller. Since the exerted force makes the pitch deflection angle exceed the threshold $\Delta\theta_{th} = 3\ deg$ (whose value is determined from the characterization of the pitch angle noise), the Z-axis reference is modified to decrease the altitude so the multi-rotor pose is accommodated to the human intention. Once the pitch deflection angles is under the threshold again, the dead-zone function ceases the integration so the reference remains constant. Five consecutive tests were conducted in which the user reduced the height of the basket by exerting a pushing force downwards against the basket. The altitude of the platform was restored by a human pilot between the tests.

On the other hand, Figs. 22 and 23 show the reaction of the compliant controller when the human user pulls the platform laterally. Note that forces exerted on the basket along the $\mathbf{Y_B}$ axis tend to cause moments in yaw that may result in uncomfortable poses for the user, so it is preferred to adapt the position of the multi-rotor in this axis to maintain constant the heading during the delivery.

6.5 Complete Operation

The complete through-window home aerial delivery operation (see Fig. 1) was validated in the same indoor testbed scenario in order to have an overall estimation of the involved time, although without considering the outdoor navigation phase. In this scenario, the supply point with the LiCAS and the user's window are located at 2 and 3 m distance in the X and Y axes from the take-off position, respectively. The trajectory followed by the FAMR is represented in Figs. 24 and 25. The execution of the experiment can be seen in

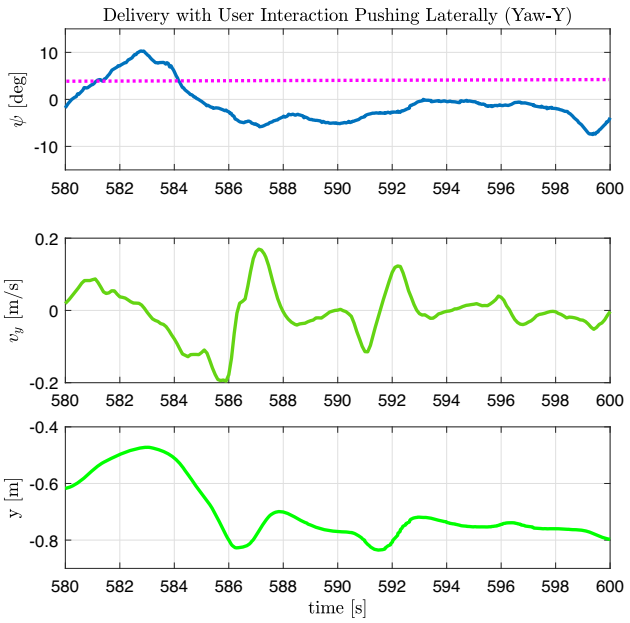

Fig. 23 FAMR yaw angle, Y-axis speed and position when the human user exerts a lateral pushing force on the basket

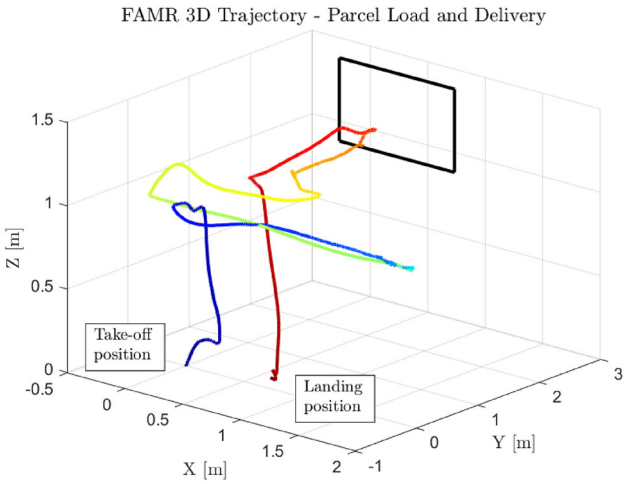

Fig. 24 FAMR 3D trajectory followed during the complete parcel load, transportation, and delivery in the indoor scenario

the video attachment. The take-off and parcel load phases are executed in 45 s, whereas the approaching to the user's window and parcel delivery is conducted in 30 s. The performance time can be improved around 20–30% by increasing the flight speed and reducing the time interval between waypoints during the approaching maneuvers.

7 Conclusion and Future Work

This paper presented an aerial delivery system consisting of a lightweight and compliant anthropomorphic dual arm manipulator used to load small parcels in the front basket of a fully actuated multi-rotor that conducts the delivery operation directly to the users' home through the window of his/her building, so the parcel can be comfortably and quickly retrieved, overcoming the limitations of ground robots navigating in dense urban environments. Identification experiments evidence that the FAMR suffers a significant displacement in the pitch angle and in the forward direction (up to 1 m for a 120 gs payload) when the parcel is loaded/unloaded from the basket due to the mass unbalance, which motivates the use of a compliant dual arm for holding the base of the basket with one of the arms while the parcel is dropped in the basket with the other arm, preventing in this way possible impacts of the platform against the manipulator in the supply area.

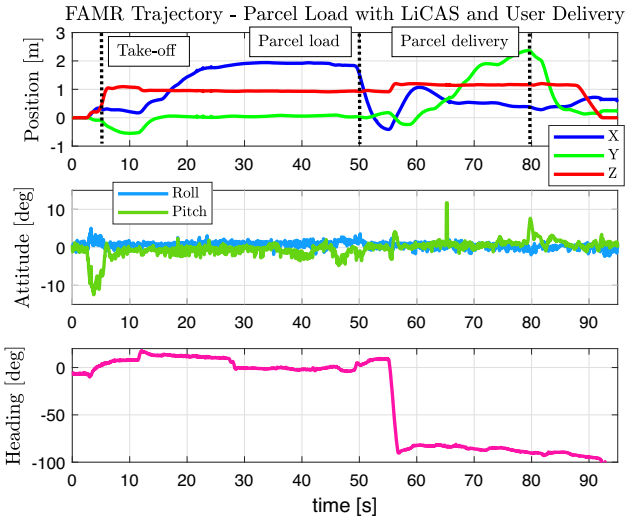

Fig. 25 Evolution of the FAMR position and attitude during the realization of the complete parcel load and delivery operation

The ability of fully actuated multi-rotors to decouple the translational and rotational motion was exploited here, incorporating a modified admittance controller over the position-attitude cascade controller so the user can guide manually the platform by interpreting the pose control errors as Cartesian and joint deflection values caused by the external contact forces. The robustness and reliability of the cascade position-attitude control scheme implemented by most autopilots is experimentally evaluated through the application of impulsive and pushing forces while the platform is hovering at a fixed position. Qualitatively, the user perceives a feeling of safety during close interaction thanks to the carbon fiber protection panel that separates the basket from the propellers, and due to the decoupled position and attitude control that prevents forward position displacements when tilting moments are exerted over the platform. Experimental results in a representative indoor scenario with an Opti-Track

positioning system validate the complete operation, providing some time metrics to evaluate the system performance.

The future work should be focused in three main aspects in order to advance towards the real application outdoors of the proposed system. First, the effect of wind should be evaluated to ensure that this can be supported without affecting significantly the positioning accuracy and reliability of the platform, involving the incorporation of wind speed measurement and estimation methods, and the adoption of control modes more suitable to overcome this perturbation. Second, the payload-to-weight ratio of the aerial platform should be improved, and, more specifically, the miniaturization and integration of the electronics, sensors, and the rest of onboard components is essential to achieve a significant weight reduction to increase safety when flying in urban areas. Finally, users' surveys, ethical and regulation aspects have to be considered towards the practical application in urban or rural environments of the proposed home aerial delivery system.

Acknowledgements This work is supported by the European ROBotics and AI Network (euROBIN, Grant Agreement ID: 101070596) and the AEROTRAIN Marie Skłodowska-Curie (MSCA-ITN-2020-953454) Projects, funded by the European Commission. The research work of Alejandro Suarez was supported by the Consejería de Transformación Económica, Industria, Conocimiento y Universidades de la Junta de Andalucía (Spain) through a post-doctoral research Grant.

Funding Funding for open access publishing: Universidad de Sevilla/CBUA.

References

1. Scott JE, Scott CH (2020) Drone delivery models for medical emergencies. In: Delivering superior health and wellness management with IoT and analytics, pp 69–85
2. Hii MSY, Courtney P, Royall PG (2019) An evaluation of the delivery of medicines using drones. Drones 3(3):52
3. Ghelichi Z, Gentili M, Mirchandani PB (2021) Logistics for a fleet of drones for medical item delivery: a case study for Louisville, KY. Comput Oper Res 135:105443
4. Czeisler MÉ, Marynak K, Clarke KE, Salah Z, Shakya I, Thierry JM, Ali N, McMillan H, Wiley JF, Weaver MD et al (2020) Delay or avoidance of medical care because of covid-19-related concerns-United States, June 2020. Morb Mortal Wkly Rep 69(36):1250
5. Boysen N, Fedtke S, Schwerdfeger S (2021) Last-mile delivery concepts: a survey from an operational research perspective. OR Spectrum 43:1–58
6. Cordts M, Omran M, Ramos S, Rehfeld T, Enzweiler M, Benenson R, Franke U, Roth S, Schiele B (2016) The cityscapes dataset for semantic urban scene understanding. In: Proceedings of the IEEE conference on computer vision and pattern recognition, pp 3213–3223
7. Yin J, Li A, Li T, Yu W, Zou D (2021) M2dgr: a multi-sensor and multi-scenario slam dataset for ground robots. IEEE Robot Autom Lett 7(2):2266–2273
8. Trautman P, Ma J, Murray RM, Krause A (2015) Robot navigation in dense human crowds: statistical models and experimental studies of human–robot cooperation. Int J Robot Res 34(3):335–356
9. Charalampous K, Kostavelis I, Gasteratos A (2017) Recent trends in social aware robot navigation: a survey. Robot Auton Syst 93:85–104
10. Klemm V, Morra A, Salzmann C, Tschopp F, Bodie K, Gulich L, Küng N, Mannhart D, Pfister C, Vierneisel M et al: (2019) Ascento: a two-wheeled jumping robot. In: 2019 International conference on robotics and automation (ICRA), pp 7515–7521. IEEE
11. Liu L, Dugas D, Cesari G, Siegwart R, Dubé R (2020) Robot navigation in crowded environments using deep reinforcement learning. In: 2020 IEEE/RSJ international conference on intelligent robots and systems (IROS), pp 5671–5677. IEEE
12. Heiden E, Palmieri L, Bruns L, Arras KO, Sukhatme GS, Koenig S (2021) Bench-mr: a motion planning benchmark for wheeled mobile robots. IEEE Robot Autom Lett 6(3):4536–4543
13. Miki T, Lee J, Hwangbo J, Wellhausen L, Koltun V, Hutter M (2022) Learning robust perceptive locomotion for quadrupedal robots in the wild. Sci Robot 7(62):2822
14. Brunner G, Szebedy B, Tanner S, Wattenhofer R (2019) The urban last mile problem: autonomous drone delivery to your balcony. In: 2019 International conference on unmanned aircraft systems (ICUAS), pp 1005–1012. IEEE
15. Das DN, Sewani R, Wang J, Tiwari MK (2020) Synchronized truck and drone routing in package delivery logistics. IEEE Trans Intell Transp Syst 22(9):5772–5782
16. Di Puglia Pugliese L, Macrina G, Guerriero F (2021) Trucks and drones cooperation in the last-mile delivery process. Networks 78(4):371–399
17. Augugliaro F, D'Andrea R (2013) Admittance control for physical human–quadrocopter interaction. In: 2013 European control conference (ECC), pp 1805–1810. IEEE
18. Suarez A, Salmoral R, Garofano-Soldado A, Heredia G, Ollero A (2022) Aerial device delivery for power line inspection and maintenance. In: 2022 International conference on unmanned aircraft systems (ICUAS), pp 30–38. IEEE
19. Suarez A, Real F, Vega VM, Heredia G, Rodriguez-Castaño A, Ollero A (2020) Compliant bimanual aerial manipulation: standard and long reach configurations. IEEE Access 8:88844–88865
20. Tognon M, Alami R, Siciliano B (2021) Physical human–robot interaction with a tethered aerial vehicle: application to a force-based human guiding problem. IEEE Trans Robot 37(3):723–734
21. Afifi A, Holland M, Franchi A (2022) Toward physical human–robot interaction control with aerial manipulators: compliance, redundancy resolution, and input limits. In: 2022 International conference on robotics and automation (ICRA), pp 4855–4861. IEEE
22. Staub N, Mohammadi M, Bicego D, Delamare Q, Yang H, Prattichizzo D, Giordano PR, Lee D, Franchi A (2018) The telemagmas: an aerial-ground comanipulator system. IEEE Robot Autom Mag 25(4):66–75
23. Sinnemann J, Boshoff M, Dyrska R, Leonow S, Mönnigmann M, Kuhlenkötter B (2022) Systematic literature review of applications and usage potentials for the combination of unmanned aerial vehi-

cles and mobile robot manipulators in production systems. Prod Eng Res Dev 16(5):579–596
24. Arbanas B, Ivanovic A, Car M, Haus T, Orsag M, Petrovic T, Bogdan S (2016) Aerial-ground robotic system for autonomous delivery tasks. In: 2016 IEEE international conference on robotics and automation (ICRA), pp 5463–5468. IEEE
25. Watkins S, Burry J, Mohamed A, Marino M, Prudden S, Fisher A, Kloet N, Jakobi T, Clothier R (2020) Ten questions concerning the use of drones in urban environments. Build Environ 167:106458
26. Son CY, Seo H, Jang D, Kim HJ (2020) Real-time optimal trajectory generation and control of a multi-rotor with a suspended load for obstacle avoidance. IEEE Robot Autom Lett 5(2):1915–1922. https://doi.org/10.1109/LRA.2020.2967279
27. Klausen K, Meissen C, Fossen TI, Arcak M, Johansen TA (2018) Cooperative control for multirotors transporting an unknown suspended load under environmental disturbances. IEEE Trans Control Syst Technol 28(2):653–660
28. Faust A, Palunko I, Cruz P, Fierro R, Tapia L (2017) Automated aerial suspended cargo delivery through reinforcement learning. Artif Intell 247:381–398
29. Guo D, Leang KK (2020) Image-based estimation, planning, and control of a cable-suspended payload for package delivery. IEEE Robot Autom Lett 5(2):2698–2705
30. Ackerman E, Koziol M (2019) The blood is here: zipline's medical delivery drones are changing the game in Rwanda. IEEE Spectr 56(5):24–31
31. Mittal M, Mohan R, Burgard W, Valada A (2022) Vision-based autonomous UAV navigation and landing for urban search and rescue. In: Robotics research: the 19th international symposium ISRR, pp 575–592. Springer
32. Koh CH, Low K, Li L, Zhao Y, Deng C, Tan SK, Chen Y, Yeap BC, Li X (2018) Weight threshold estimation of falling UAVs (unmanned aerial vehicles) based on impact energy. Transp Res Part C Emerg Technol 93:228–255
33. Cour-Harbo A (2017) Mass threshold for 'harmless' drones. Int J Micro Air Veh 9(2):77–92
34. Tomic T, Schmid K, Lutz P, Domel A, Kassecker M, Mair E, Grixa IL, Ruess F, Suppa M, Burschka D (2012) Toward a fully autonomous UAV: research platform for indoor and outdoor urban search and rescue. IEEE Robot Autom Mag 19(3):46–56
35. Kong F, Xu W, Cai Y, Zhang F (2021) Avoiding dynamic small obstacles with onboard sensing and computation on aerial robots. IEEE Robot Autom Lett 6(4):7869–7876
36. Liu X, Li G, Loianno G (2022) Safety-aware human-robot collaborative transportation and manipulation with multiple MAVs. arXiv preprint arXiv:2210.05894
37. Saunders J, Saeedi S, Li W (2021) Autonomous aerial delivery vehicles, a survey of techniques on how aerial package delivery is achieved. arXiv preprint arXiv:2110.02429
38. Meng J, Buzzatto J, Liu Y, Liarokapis M (2022) On aerial robots with grasping and perching capabilities: a comprehensive review. Front Robot AI 405
39. Ollero A, Tognon M, Suarez A, Lee D, Franchi A (2021) Past, present, and future of aerial robotic manipulators. IEEE Trans Robot 38(1):626–645
40. Lindsey Q, Mellinger D, Kumar V (2012) Construction with quadrotor teams. Auton Robot 33(3):323–336
41. Kornatowski PM, Feroskhan M, Stewart WJ, Floreano D (2020) Downside up: rethinking parcel position for aerial delivery. IEEE Robot Autom Lett 5(3):4297–4304
42. Maki T, Zhao M, Shi F, Okada K, Inaba M (2020) Model reference adaptive control of multirotor for missions with dynamic change of payloads during flight. In: 2020 IEEE international conference on robotics and automation (ICRA), pp 7433–7439. https://doi.org/10.1109/ICRA40945.2020.9196861
43. Lee S, Son H (2021) Antisway control of a multirotor with cable-suspended payload. IEEE Trans Control Syst Technol 29(6):2630–2638. https://doi.org/10.1109/TCST.2020.3035004
44. Pounds PEI, Deer W (2018) The safety rotor-an electromechanical rotor safety system for drones. IEEE Robot Autom Lett 3(3):2561–2568. https://doi.org/10.1109/LRA.2018.2811842
45. Hamandi M, Usai F, Sablé Q, Staub N, Tognon M, Franchi A (2021) Design of multirotor aerial vehicles: a taxonomy based on input allocation. Int J Robot Res 40(8–9):1015–1044
46. Rajappa S, Ryll M, Bülthoff HH, Franchi A (2015) Modeling, control and design optimization for a fully-actuated hexarotor aerial vehicle with tilted propellers. In: 2015 IEEE international conference on robotics and automation (ICRA), pp 4006–4013. IEEE
47. Ryll M, Muscio G, Pierri F, Cataldi E, Antonelli G, Caccavale F, Franchi A (2017) 6D physical interaction with a fully actuated aerial robot. In: 2017 IEEE international conference on robotics and automation (ICRA), pp 5190–5195. IEEE
48. Ghadiok V, Goldin J, Ren W (2011) Autonomous indoor aerial gripping using a quadrotor. In: 2011 IEEE/RSJ international conference on intelligent robots and systems, pp 4645–4651. IEEE
49. Maier M, Oeschger A, Kondak K (2015) Robot-assisted landing of VTOL UAVs: design and comparison of coupled and decoupling linear state-space control approaches. IEEE Robot Autom Lett 1(1):114–121
50. Xu R, Ji X, Hou J, Liu H, Qian H (2021) A predictive control method for stabilizing a manipulator-based UAV landing platform on fluctuating marine surface. In: 2021 IEEE/RSJ international conference on intelligent robots and systems (IROS), pp 8625–8632. IEEE
51. Suarez A, Heredia G, Ollero A (2018) Design of an anthropomorphic, compliant, and lightweight dual arm for aerial manipulation. IEEE Access 6:29173–29189
52. Suarez A, Jimenez-Cano AE, Vega VM, Heredia G, Rodriguez-Castaño A, Ollero A (2018) Design of a lightweight dual arm system for aerial manipulation. Mechatronics 50:30–44
53. Suarez A, Heredia G, Ollero A (2018) Physical-virtual impedance control in ultralightweight and compliant dual-arm aerial manipulators. IEEE Robot Autom Lett 3(3):2553–2560
54. Suarez A, Sanchez-Cuevas PJ, Heredia G, Ollero A (2020) Aerial physical interaction in grabbing conditions with lightweight and compliant dual arms. Appl Sci 10(24):8927
55. Robinson N, Tidd B, Campbell D, Kulić D, Corke P (2023) Robotic vision for human-robot interaction and collaboration: a survey and systematic review. ACM Trans Human Robot Interact 12(1):1–66
56. Haddadin S, Croft E (2016) Physical human–robot interaction. In: Springer handbook of robotics, pp 1835–1874
57. Yen B, Li Y, Hioka Y (2023) Rotor noise-aware noise covariance matrix estimation for unmanned aerial vehicle audition. In: IEEE/ACM transactions on audio, speech, and language processing
58. Abioye A (2023) Multimodal speech and visual gesture control interface technique for small unmanned multirotor aircraft. PhD thesis, University of Southampton
59. Hu B, Wang J (2020) Deep learning based hand gesture recognition and UAV flight controls. Int J Autom Comput 17(1):17–29
60. Liu C, Szirányi T (2021) Real-time human detection and gesture recognition for on-board UAV rescue. Sensors 21(6):2180
61. Patrona F, Mademlis I, Pitas I (2021) An overview of hand gesture languages for autonomous UAV handling. In: 2021 Aerial robotic systems physically interacting with the environment (AIRPHARO), pp 1–7
62. Li T, Liu J, Zhang W, Ni Y, Wang W, Li Z (2021) UAV–human: a large benchmark for human behavior understanding with unmanned aerial vehicles. In: Proceedings of the IEEE/CVF conference on computer vision and pattern recognition, pp 16266–16275

63. Alami R, Albu-Schäffer A, Bicchi A, Bischoff R, Chatila R, De Luca A, De Santis A, Giralt G, Guiochet J, Hirzinger G et al: (2006) Safe and dependable physical human–robot interaction in anthropic domains: state of the art and challenges. In: 2006 IEEE/RSJ international conference on intelligent robots and systems, pp 1–16. IEEE
64. Nascimento TP, Saska M (2019) Position and attitude control of multi-rotor aerial vehicles: a survey. Annu Rev Control 48:129–146
65. European Robotics and AI Network Homepage. https://www.eurobin-project.eu/
66. Jedsy Homepage, Delivery Drone Capable of Perching on Windows. https://jedsy.com/
67. Rashad R, Goerres J, Aarts R, Engelen JB, Stramigioli S (2020) Fully actuated multirotor UAVs: a literature review. IEEE Robot Autom Mag 27(3):97–107
68. Bahabry A, Wan X, Ghazzai H, Menouar H, Vesonder G, Massoud Y (2019) Low-altitude navigation for multi-rotor drones in urban areas. IEEE Access 7:87716–87731
69. Gyagenda N, Hatilima JV, Roth H, Zhmud V (2022) A review of GNSS-independent UAV navigation techniques. Robot Auton Syst 152:104069
70. Park G, Lee B, Kim DG, Lee YJ, Sung S (2020) Design and performance validation of integrated navigation system based on geometric range measurements and GIS map for urban aerial navigation. Int J Control Autom Syst 18(10):2509–2521
71. Rajappa S, Bülthoff HH, Odelga M, Stegagno P (2017) A control architecture for physical human–UAV interaction with a fully actuated hexarotor. In: 2017 IEEE/RSJ international conference on intelligent robots and systems (IROS), pp 4618–4625. IEEE
72. Corsini G, Jacquet M, Das H, Afifi A, Sidobre D, Franchi A (2022) Nonlinear model predictive control for human-robot handover with application to the aerial case. In: 2022 IEEE/RSJ international conference on intelligent robots and systems (IROS), pp 7597–7604. IEEE
73. Oudah M, Al-Naji A, Chahl J (2020) Hand gesture recognition based on computer vision: a review of techniques. J Imaging 6(8):73
74. Romero-Ramirez FJ, Muñoz-Salinas R, Medina-Carnicer R (2018) Speeded up detection of squared fiducial markers. Image Vis Comput 76:38–47
75. Lemardelé C, Estrada M, Pagès L, Bachofner M (2021) Potentialities of drones and ground autonomous delivery devices for last-mile logistics. Transp Res Part E Logist Transp Rev 149:102325
76. Sanchez-Cuevas PJ, Gonzalez-Morgado A, Cortes N, Gayango DB, Jimenez-Cano AE, Ollero A, Heredia G (2020) Fully-actuated aerial manipulator for infrastructure contact inspection: design, modeling, localization, and control. Sensors. https://doi.org/10.3390/s20174708
77. Authority CAS (2013) Human injury model for small unmanned aircraft impacts. Monash University, Melbourne, Australia
78. Balestrieri E, Daponte P, De Vito L, Picariello F, Tudosa I (2021) Sensors and measurements for UAV safety: an overview. Sensors 21(24):8253
79. Hedayati H, Suzuki R, Leithinger D, Szafir D (2020) Pufferbot: actuated expandable structures for aerial robots. In: 2020 IEEE/RSJ international conference on intelligent robots and systems (IROS), pp 1338–1343. IEEE
80. Plioutsias A, Karanikas N, Chatzimihailidou MM (2018) Hazard analysis and safety requirements for small drone operations: To what extent do popular drones embed safety? Risk Anal 38(3):562–584
81. Tognon M, Franchi A (2018) Omnidirectional aerial vehicles with unidirectional thrusters: theory, optimal design, and control. IEEE Robot Autom Lett 3(3):2277–2282
82. Sanchez-Cuevas PJ, Gonzalez-Morgado A, Cortes N, Gayango DB, Jimenez-Cano AE, Ollero A, Heredia G (2020) Fully-actuated aerial manipulator for infrastructure contact inspection: design, modeling, localization, and control. Sensors 20(17):4708
83. Albu-Schäffer A, Ott C, Hirzinger G (2007) A unified passivity-based control framework for position, torque and impedance control of flexible joint robots. Int J Robot Res 26(1):23–39
84. Pratt GA, Williamson MM (1995) Series elastic actuators. In: Proceedings 1995 IEEE/RSJ international conference on intelligent robots and systems. Human robot interaction and cooperative robots, vol 1, pp 399–406. IEEE
85. Kotaru P, Edmonson R, Sreenath K (2020) Geometric l1 adaptive attitude control for a quadrotor unmanned aerial vehicle. J Dyn Syst Meas Contr 142(3):031003
86. Zhao J, Ding X, Jiang B, Jiang G, Xie F (2021) A novel control strategy for quadrotors with variable mass and external disturbance. Int J Robust Nonlinear Control 31(17):8605–8631
87. Xie W, Cabecinhas D, Cunha R, Silvestre C (2021) Adaptive backstepping control of a quadcopter with uncertain vehicle mass, moment of inertia, and disturbances. IEEE Trans Ind Electron 69(1):549–559
88. Zhou L, Xu S, Jin H, Jian H (2021) A hybrid robust adaptive control for a quadrotor UAV via mass observer and robust controller. Adv Mech Eng 13(3):16878140211002724
89. LiCAS A1–AC1 Teleoperation Leader-Follower. https://www.youtube.com/watch?v=XCYpS1w_diM